Available online at www.sciencedirect.com

SCIENCE DIRECT

Developmental Biology 285 (2005) 138 – 155

DEVELOPMENTAL BIOLOGY

www.elsevier.com/locate/ydbio

Mutations that affect the survival of selected amacrine cell subpopulations define a new class of genetic defects in the vertebrate retina

Andrei Avanesov[a], Ralf Dahm[b], The Tuebingen 2000 Screening Consortium[1], William F. Sewell[c], Jarema J. Malicki[a,*]

[a]*Department of Ophthalmology, Harvard Medical School/MEEI, 243 Charles Street, Boston, MA 02114, USA*
[b]*Max Planck Institut fur Entwicklungsbiologie, Abteilung III/Genetik, Spemannstrasse 35, 72076 Tubingen, Germany*
[c]*Department of Otolaryngology, Harvard Medical School/MEEI, 243 Charles Street, Boston, MA 02114, USA*

Received for publication 7 October 2004, revised 25 May 2005, accepted 8 June 2005

Abstract

Amacrine neurons are among the most diverse cell classes in the vertebrate retina. To gain insight into mechanisms vital to the production and survival of amacrine cell types, we investigated a group of mutations in three zebrafish loci: *kleks* (*kle*), *chiorny* (*chy*), and *bergmann* (*bgm*). Mutants of all three genes display a severe loss of selected amacrine cell subpopulations. The numbers of GABA-expressing amacrine interneurons are sharply reduced in all three mutants, while cell loss in other amacrine cell subpopulations varies and some cells are not affected at all. To investigate how amacrine cell loss affects retinal function, we performed electroretinograms on mutant animals. While the *kle* mutation mostly influences the function of the inner nuclear layer, unexpectedly the *chy* mutant phenotype also involves a loss of photoreceptor cell activity. The precise ratios and arrangement of amacrine cell subpopulations suggest that cell–cell interactions are involved in the differentiation of this cell class. To test whether defects of such interactions may be, at least in part, responsible for mutant phenotypes, we performed mosaic analysis and demonstrated that the loss of parvalbumin-positive amacrine cells in *chy* mutants is due to extrinsic (cell-nonautonomous) causes. The phenotype of another amacrine cell subpopulation, the GABA-positive cells, does not display a clear cell-nonautonomy in *chy* animals. These results indicate that environmental factors, possibly interactions among different subpopulations of amacrine neurons, are involved in the development of the amacrine cell class.

Keywords: Zebrafish; Retina; Electroretinogram; Amacrine neuron; Degeneration; Cell fate; Cell death; Neurotrophins

Introduction

The vertebrate retina is a complex neuronal network that plays an essential role in visual perception. During embryonic development, the retinal neuroepithelium gives rise to six major classes of neurons and the Mueller glia. Nearly all retinal cell classes consist of morphologically distinct subpopulations. This diversity is particularly pronounced in the amacrine cell layer. In the mammalian retina, based on their morphology, cells of this class have been grouped into nearly 30 distinct types, which are present in defined ratios and distribute in a nonrandom manner in the plane of the inner nuclear layer (MacNeil and Masland, 1998; MacNeil et al., 1999). In addition to morphology, cell diversity in the amacrine cell layer is apparent in the

* Corresponding author. Fax: +1 617 573 4290.
E-mail address: jarema_malicki@meei.harvard.edu (J.J. Malicki).

[1] F. van Bebber, E. Busch-Nentwich, R. Dahm, H.-G. Frohnhofer, H. Geiger, D. Gilmour, S. Holley, J. Hooge, D. Julich, F. Maderspacher, H.-M. Maischein, C. Neumann, T. Nicolson, C. Nusslein-Volhard, H. Roehl, U. Schonberger, C. Seiler, C. Sollner, M. Sonawane, A. Wehner, and C. Weiler (Max Planck Institut fur Entwicklungsbiologie, Abteilung III/Genetik, Spemannstrasse 35, 72076 Tubingen, Germany); P. Erker, H. Habeck, U. Hagner, C.E. Hennen Kaps, A. Kirchner, T. Koblizek, U. Langheinrich, C. Loeschke, C. Metzger, R. Nordin, J. Odenthal, M. Pezzuti, K. Schlombs, J. deSantana-Stamm, T. Trowe, G. Vacun, B. Walderich, A. Walker, and C. Weiler (Artemis Pharmaceuticals GmbH, an Exelixis Company, Spemannstrasse 35, 72076 Tubingen, Germany).

0012-1606/$ - see front matter © 2005 Elsevier Inc. All rights reserved.
doi:10.1016/j.ydbio.2005.06.009

distribution of numerous neurotransmitters or neuropeptides, which are frequently confined to a subset of amacrine neurons (reviewed in Kolb, 1997).

What are the molecular mechanisms that underlie amacrine cell diversity and the regular organization of these neurons? A number of genes have been shown to play a role in the determination of cell class identity in the vertebrate retina (for recent reviews see Livesey and Cepko, 2001; Ohnuma and Harris, 2003). Amacrine cell identity is regulated by a cooperative interaction of numerous transcriptional regulators, including Math3, Math5, NeuroD, Foxn4, and Pax6 (Dyer and Cepko, 2000; Li et al., 2004; Marquardt et al., 2001; Morrow et al., 1999). A more subtle regulatory activity in the amacrine cell layer is mediated by the cyclin kinase inhibitor, $p57^{kip2}$: its loss-of-function causes an increase of calbindin-positive cells, while other amacrine cell subpopulations investigated so far remain unaffected (Dyer and Cepko, 2000). Following their specification, amacrine cell perikarya distribute in the plane of the inner nuclear layer in a nonrandom fashion. The analysis of this distribution suggests repulsive interactions between cells of the same type (Cameron and Carney, 2000; Galli-Resta et al., 1997). Cell–cell signaling in the amacrine cell layer is also suggested by cell ablation experiments, which show that a selective loss of a specific cell population leads to its overproduction during later stages of neurogenesis (Reh, 1987; Reh and Tully, 1986).

In addition to early developmental cell–cell interactions, which may regulate the position of cell perikarya, amacrine cells interact with each other via chemical and electrical synaptic junctions (reviewed in Kolb, 1997; Vaney, 1999). These interactions may also play a role in developmental processes such as the regulation of cell numbers and cell distribution. In addition, work in several laboratories has suggested that the survival of amacrine neurons depends on trophic factors such as brain-derived neurotrophic factor (BDNF), its receptors, such as trkB, as well as insulin growth factors I and II (IGF-I, IGF-II). Following antisense knock-down of TrkB expression in murine retina, for example, the number of parvalbumin expressing amacrine cells is reduced (Rickman and Rickman, 1996). Similarly, the inhibition of BDNF in a retinal culture assay affects the survival of neurons in the amacrine cell layer (Cusato et al., 2002). Finally, in vitro studies have demonstrated that increasing the concentration of IGF-I or IGF-II in culture medium promotes the differentiation and survival of cultured rat amacrine neurons (Politi et al., 2001). Despite these advances, the genetic mechanisms that regulate amacrine cell diversity and distribution remain largely unexplored.

One productive approach to further investigate genetic pathways that regulate the differentiation and survival of amacrine cells is the analysis of mutant strains that display defects in this cell population. Unfortunately, few mutants of amacrine cell development have been isolated so far. Zebrafish, a relatively recent vertebrate model of eye development, has been effectively used to isolate genetic defects (reviewed in Malicki, 2000). Mutations in more than 30 loci, for example, have been shown to affect different stages of photoreceptor development or survival (reviewed in Tsujikawa and Malicki, 2004b). Genetic approaches in zebrafish benefit from thorough morphological and histological studies of wild-type retinal development (reviewed in Avanesov and Malicki, 2004). Genetic screens in zebrafish should thus provide an effective way to isolate mutations in amacrine cell development.

During a large-scale mutagenesis screen of 3233 genomes, we recovered 109 mutant strains characterized by defects in the neural retina. Several of these display a severe loss of cells in the inner portion of the INL, an area predominantly occupied by amacrine cell somata. Here, we provide a comprehensive phenotypic analysis of 4 mutant strains that contain defects in three loci, *kleks* (*kle*), *chiorny* (*chy*), and *bergmann* (*bgm*). We show that, in all 4 mutant lines, amacrine cell loss is largely restricted to GABA- and parvalbumin-positive neurons, and that in at least one line, the phenotype of parvalbumin-positive cells is due to cell nonautonomous causes. To our knowledge, selective loss of amacrine neuron subpopulations has not been reported in the vertebrate retina so far, and thus the mutant strains described in this study provide a valuable opportunity to gain insight into mechanisms that control the differentiation and survival of this cell class.

Materials and methods

Fish breeding and mutagenesis

Zebrafish strains were bred in standard fish facility conditions as described previously (Kimmel et al., 1995; Westerfield, 2000). ENU mutagenesis was performed on Tuebingen males using standard protocols (Mullins et al., 1994; Pelegri, 2002; Solnica-Krezel et al., 1994). Following ENU treatment and standard test crosses, males were mated to wild-type Tuebingen females and the F1 progeny originating from these crosses were raised to adulthood. F2 families were produced by in-crossing of F1 animals as described previously (Driever et al., 1996; Haffter et al., 1996).

Screening procedures

Screening was performed on F3 generation larvae obtained by in-crossing of individuals from F2 families. F3 embryos were collected in 90 mm petri dishes (Greiner, Germany) and kept at 28°C in egg water containing 0.001% (w/v) of methylene blue (Sigma, St. Louis, MO). For phenotypic observations, larvae were anesthetized in 0.02% Tricaine (Sigma) in egg water and visually inspected for externally visible phenotypes at 5 dpf using a dissecting microscope. The criteria used to screen included: externally

visible eye phenotypes, such as the size, shape, and position of the eye; the appearance of eye pigmentation; the size and shape of the pupil; the size, shape, and position of the lens, lens opacities (cataracts), and the thickness, shape, and transparency of the cornea as well as abnormally dark melanophores (as an indicator of reduced visual ability in zebrafish). Candidate mutant individuals were fixed in 4% paraformaldehyde (PFA) (w/v) in PBS and stored for further histological analysis (see histology). For each set of putative mutants, a wild-type sibling was processed in parallel as a reference. All crosses that led to the identification of mutant phenotypes were repeated to confirm reproducibility. Carriers of mutant alleles were out-crossed to wild-type Tuebingen and WIK strains for further analysis. Complementation testing was performed between heterozygous carriers of mutations falling into the same phenotypic categories.

Histology

Zebrafish larvae were raised to the desired age and processed for histological studies using JB4 embedding medium as described previously (Doerre and Malicki, 2001; Pujic and Malicki, 2001). Sections were examined using an Axioscope Microscope (Zeiss, Thornwood, NY), and DIC images were collected using an AxioCam (Zeiss). Image files were processed using Photoshop 7.0 (Adobe Systems, San Jose, CA).

Immunohistochemistry

Embryos were fixed in 4% PFA in PBS (w/v, pH 7.4) for 2–3 h at room temperature, washed twice in PBST (PBS with 0.1% Tween 20) for 5 min, infiltrated in 30% sucrose (w/v) in PBST overnight at 4°C, and embedded in molds containing OCT freezing medium (Richard-Allan Scientific, Kalamazoo, MI). Blocks were then frozen at −20°C and sectioned at 14–35 μm on a Microm HM 500 OH cryostat (Richard-Allan Scientific). Sections were collected on Superfrost Plus slides (Fisher, Pittsburgh, PA), air dried for 30 min, and re-hydrated in PBST for 10 min. For choline acetyltransferase and serotonin immunolabeling, slides were incubated in 10 mM sodium citrate, pH 6.0, at 100°C for 10 min, washed twice in PBST, 5 min each, and blocked in the blocking reagent containing 10% (v/v) normal donkey serum (Jackson Laboratories, Westgrove, PA) and 0.5% Triton X-100 (v/v) in PBST for 30 min at room temperature. For the remaining antibodies, sodium citrate treatment was omitted, and donkey serum in blocking solution was replaced with the same amount of normal goat serum (Gibco, Carlsbad, CA). Following blocking, primary antibodies were diluted in appropriate blocking solution and applied either for 2 h at room temperature or overnight at 4°C in a humidified chamber. Subsequently, sections were washed once in PBST for 10 min and incubated with fluorophore-conjugated secondary antibodies diluted 1:500 in appropriate blocking solution (1 to 2 h, room temperature). Finally, sections were washed in PBST as above, stained with YoPro nuclear marker to aid in the detection of mutant phenotypes (1:5000 dilution in PBST; Molecular Probes, Eugene, OR), coversliped in PBST, and immediately analyzed on a Leica SP2 confocal microscope (Heidelberg, Germany). GABA immunolabeling was carried out on plastic sections which were prepared as described above in the histology section with the following modifications: embryos were fixed in 2% gluteraldehyde, 2% paraformaldehyde in 0.1 M phosphate buffer (pH 7.3) for 6 h at room temperature. To aid in the selection of mutant retinae, GABA-labeled sections were counterstained with Hoechst 33258 nuclear dye (1:100,000 dilution in PBST; Molecular Probes) and then imaged on Zeiss Axioscope using UV illumination. To adjust contrast and background levels, images were processed using Photoshop software (Adobe).

The following primary antibodies and dilutions were used: anti-carbonic anhydrase (1:250; gift from Paul Linser, Whitney Laboratory, St. Augustine, FL); anti-BDNF (1:250, Santa Cruz Biotechnlogy, Santa Cruz, CA); anti-choline acetyltransferase (1:30; Chemicon, Temecula, CA); anti-GABA (1:500; Sigma); anti-human neuronal protein HuC/HuD (Hu) (1:20; Molecular Probes); anti-neuropeptide Y (1:1000; ImmunoStar, Hudson, WI); anti-parvalbumin (1:500; Chemicon); anti-serotonin (1:250; Sigma); anti-TrkB (1:250, Santa Cruz Biotechnology); anti-TrkC (1:250 Santa Cruz Biotechnology); anti-tyrosine hydroxylase (1:100; Chemicon); and Zpr-1 (1:150; Oregon Monoclonal Bank, Eugene, OR). The specificity of BDNF and Trk antibodies was tested by including blocking peptides (provided by Santa Cruz Biotechnology) in primary antibody solution at the concentration of ca. 0.8 μg/ml.

Analysis of CA-, ChAt-, NPY-, Pv-, Ser-, TH-, and Zpr-1-immunoreactive cells was performed from *z*-series stacks of 6, 12, 30, 12, 30, 30, and 12 μm, respectively. YoPro-labeled nuclei and BDNF-, TrkB-, TrkC-, and Hu-positive cells were analyzed on single confocal optical sections. GABA and Hoechst counts were performed on 5 μm plastic sections using UV illumination for Hoescht detection. In all immunostaining experiments performed at 6 dpf, for each individual, we analyzed a single section through the center of the retina, using lens size or the presence of the optic nerve as reference points. The statistical significance of cell count differences was evaluated using the Mann–Whitney *U* test, or in some cases by Student *t* test. The analysis of BDNF and TrkB expression was carried out on embryos derived from crosses between heterozygous carries of mutant alleles, roughly at the time when mutant phenotypes become first detectable on plastic sections (4 dpf for *chy*, and 5 dpf for *kle* and *brg*). As mutants cannot be reliably distinguished from wild-type animals based on the external appearance at these stages, immunohistochemical analysis was performed on 12 randomly selected individuals from each cross.

Eye surgery

Removal of eyes from zebrafish larvae was carried out as described previously (Kainz et al., 2003). Following surgery, larvae were raised to 6 dpf and genotyped on plastic sections as above. Surgically removed eyes were processed for immunohistochemistry and analyzed as above.

Cell death detection by TUNEL assay

Zebrafish larvae were fixed in 4% PFA, cryoprotected in sucrose, and sectioned as above at 14 μm. Following two washes, 10 min each, in 50 mM PBS (pH 7.4), sections were treated with Proteinase K (Roche Applied Sciences, Indianapolis, IN) for 10 min at the concentration of 2 μg/ml in 50 mM Tris–HCl buffer, pH 8. Subsequently, sections were rinsed 3 times in 50 mM Tris–HCl buffer, incubated 5 min in 70% ethanol/30% acetic acid solution at −20°C, washed 5 times, 5 min each, in 50 mM Tris–HCl buffer, and treated with blocking solution, containing (v/v in PBST) 10% normal goat serum, and 0.5% Triton X-100 (30 min, room temperature). Finally, sections were incubated with TUNEL reaction mixture (Roche) at 37°C for several hours according to manufacturer's instructions. To detect apoptotic nuclei, sections were rinsed in 50 mM PBS for 10 min, coversliped, and analyzed by confocal microscopy as above. Images were processed using Photoshop 7.0. TUNEL-positive nuclei were counted and statistical analysis was carried out using Mann–Whitney *U* test. To distinguish between amacrine cells and other INL neurons, counts were taken separately from the inner and the outer halves of the INL.

ERG measurements

For ERG recording, mutant and wild-type zebrafish larvae were raised using the light/dark cycle as above until 4–6 dpf. Recordings were performed on isolated larval eyes as described previously (Kainz et al., 2003; Wong, 2005) with the following modifications. The larvae were anesthetized in 0.01% tricaine, placed on a paper towel moistened with a modified Ringer solution containing 20 mM of glucose (Dmitriev and Mangel, 2000), and the eye was removed using a tungsten needle. The isolated eye was then placed lens side up, facing the light source. In the course of the recording session, the eye was perfused with oxygenated Ringer's solution. The light stimulus was generated by an Ace power supply (Fostec, Auburn, NY), equipped with a 100 W light bulb, and delivered to the specimen through a fiber-optic cable to which a 10× (0.25 n.a.) microscope objective was attached for focusing the light onto the eye. Light flashes of ca. 8400 μW/cm^2 were produced using an electronically controlled shutter (Uniblitz, Vincent Associates, Rochester, NY) and were attenuated over 3 orders of magnitude using gelatin neutral density filters (Kodak, Rochester, NY). To reduce electrical noise, the experiments were performed in a Faraday cage. Retinal responses were monitored with a glass micropipette (tip diameter 10 μm) filled with PBS. The signal was amplified 100× using a low noise amplifier (DL Instruments, Ithaca, NY), and bandpass-filtered with corner frequencies of 0.3 and 1000 Hz. Data were acquired using a 1 kHz sampling rate with a National Instruments IO Board (PCI 6052) and LabView 6.1 software. The stimulus duration was 800 ms and the interstimulus time 2 s. Recordings were performed on light adapted retinae using background illumination of ca. 20 μW/cm^2. Responses from mutant and wild-type siblings were alternately monitored during a single session. For each measurement, 10 consecutive responses per animal were averaged to reduce background noise. A minimum of 4 animals were used to collect each data point. The a-wave isolation was accomplished by bathing isolated eyes in 2-amino-4-phosphonobutyric acid (APB) and threo-beta-benzyloxyaspartate (TBOA) as described previously (Kainz et al., 2003; Wong, 2005). Statistical evaluation of amplitude differences was carried out using Student's *t* test.

Mosaic analysis

Blastomere transplantations were performed as described previously (Avanesov and Malicki, 2004; Ho and Kane, 1990; Pujic and Malicki, 2001). Briefly, 5% lysine-fixable biotin dextran (Molecular Probes) was purified using Microcon YM-3 Centrifugal Filters (Millipore, Bedford, MA) by spinning the columns 5 times at 10,000 *g* for 30 min. Dextran was injected into donor embryos at 1–4 cell stage, and at late blastula stage, 15–30 cells were removed from donor embryos and transferred into the animal pole of host embryos. The detection of GABA expressing donor-derived cells was performed on plastic sections. Briefly, host embryos were fixed in a mixture of formaldehyde and gluteraldehyde as described above, washed in PBSTD (PBS with 1% Triton X-100 and 1% DMSO v/v), then rinsed in water, immersed in prechilled acetone for 5 min at −20°C, washed once in water and once in PBSTD, 5 min each, and incubated in 10 μg/ml collagenase (Sigma) in PBSTD for 30 min at room temperature. Subsequently, embryos were washed several times in PBSTD and incubated with Alexa 546-conjugated streptavidin (1:200; Molecular Probes) overnight at 4°C. After 4 PBSTD washes, 15 min each, embryos were dehydrated in graded ethanol series, embedded in JB4, and sectioned as above. Finally, GABA detection was carried out as described above. The frequency of GABA-positive donor-derived cells was evaluated by confocal microscopy. Pv-positive donor-derived cells were detected on frozen sections. Mosaic embryos were fixed, cryosectioned, and processed for immunostaining using anti-parvalbumin antibody as described above. Donor-derived cells were detected using Alexa 546-conjugated streptavidin applied in blocking solution at 1:500 dilution

during the secondary antibody staining step. The frequency of donor-derived amacrine cells was evaluated as described previously for photoreceptors (Doerre and Malicki, 2001, 2002).

Electron microscopy

Zebrafish larvae were fixed overnight at 4°C in 2.5% gluteraldehyde and 2% formaldehyde in cacodylate buffer (0.1 M) containing 0.08 M $CaCl_2$. Following fixation, larvae were washed twice in cacodylate buffer for 15 min, post-fixed in 2% osmium tetroxide in cacodylate buffer for 1.5 h at room temperature, rinsed twice in cacodylate buffer for 10 min and once in water, and stained in 2% uranyl acetate in maleate buffer (Ernst F. Fullam, Schenectady, NY) for 20 min. Dehydration in graded ethanol series and embedding in Epon (Polysciences, Warrington, PA) were performed as described previously (Doerre and Malicki, 2001, 2002). 70–90 μm ultrathin sections were prepared and post-stained with aqueous uranyl acetate solution as above. Analysis was performed using Phillips CM-10 and JEOL JEM 100 CX electron microscopes.

Semi-quantitative RT-PCR

Eyes of wild-type and mutant larvae were dissected at 5–6 dpf and used to extract RNA with Trizol reagent as described in our previous work (Tsujikawa and Malicki, 2004a). RT-PCR was performed as described previously (Tsujikawa and Malicki, 2004a) using the following PCR conditions: denaturing at 95°C for 30 s, annealing at 60°C for 30 s, and extension at 72°C for 30 s for the total of 38 cycles using Ex-Taq polymerase (Takara, Inc). *β-actin* amplification served as a control for the efficiency of RNA purification procedure. The following primer pairs were used in these experiments: 5′-CCA CCA TGA AGA TCA AGA TC-3′ and 5′-GGT GGC AAC AGT TCT GTT TA-3′ for *β-actin* control; 5′-GAG CAG GTC ATT GAG GAG TT-3′ and 5′-CAG CTG TCA CCC ACT GGC TA-3′ for *bdnf*; 5′-GTT TGT GTG GAG AGC GAT CCT-3′ and 5′-CAC CAA GAG ATT TTC TCC GAC-3′ for *trkB1* (*ntrk2a*); 5′-G GAT CCC ACA CTT GCA GCA-3′ and 5′-CTG TAG CGG CTG TCC GTC AAA-3′ for *trkC1* (*ntrk3a*); 5′-GTG ATG TCT TTA AGT GTA ACC AT-3′ and 5′-CTG ATG AAC CTC CTT ACA GGA-3′ for *igf1*; 5′-ATG GAT GAT TAC CAT GTA TT-3′ and 5′-TCA TTT TCG GGA TGT GCT GA-3′ for *igf2* (Maures et al., 2002).

Results

A screen for visual system mutants

In the course of a large-scale chemical mutagenesis screen, we searched for mutants that affect visual system development. Teleost melanophores are known to redistribute their pigment granules in response to illumination changes (Fujii, 2000; Murphy and Tilney, 1974; Sugimoto, 2002). This vision-dependent response, thought to serve the purpose of background adaptation, has been also observed in zebrafish and is defective in several zebrafish retinal mutants (Malicki et al., 1996; Neuhauss et al., 1999). Taking advantage of this behavior, we identified 122 mutant strains characterized by abnormal background adaptation. The retinae of these mutant animals were subsequently inspected in plastic sections. This analysis revealed 109 mutant strains characterized by histological defects in the retina. Here, we present an analysis of four mutations that produce abnormally dark melanophore pigmentation and amacrine cell loss. All four defects segregate in a Mendelian fashion and display recessive, fully-penetrant phenotypes (summarized in Table 1). Based on complementation testing, these mutants define three loci: *kleks* (*kle*), *bergmann* (*bgm*), and *chiorny* (*chy*).

The most obvious feature of external phenotype in mutant animals is abnormally dark melanophores. In *kle*, melanophores appear excessively dark on the dorsal surface of the head and trunk by 120 hpf (hours post-fertilization) (Fig. 1C, compare to the wild type in A). As development proceeds, the pigmentation phenotype becomes more pronounced, and the *kle* mutant embryos look nearly black both dorsally and

Table 1
Summary of mutant phenotypes

Locus name	Alleles	External phenotype	Retinal phenotype
kleks (kle)	*t24734*	5 dpf: abnormally dark melanophores, swim bladder absent	6 dpf: numbers of GABA-, Pv-, and ChAt-positive amacrine cells reduced
bergmann (bgm)	*t21127*	5 dpf: abnormally dark melanophores, poor touch response, swim bladder absent	6 dpf: numbers of GABA-positive amacrine cells and bipolar cell nuclei reduced
chiorny (chy)	*t21118*	6 dpf: abnormally dark melanophores, reduced size eye and lens, poor touch response, swim bladder absent	6 dpf: numbers of GABA-, Pv-, ChAt-, and Ser-positive amacrine cells reduced. Fewer photoreceptors, Mueller glia, and bipolar cells
	t23198	6 dpf: abnormally dark melanophores, reduced size eye and lens, poor touch response, brain necrosis, swim bladder absent	6 dpf: numbers of Pv-positive amacrine cells reduced. Fewer photoreceptors and Mueller glia

ChAt, Pv, and Ser are choline acetyltransferase, parvalbumin, and serotonin, respectively.

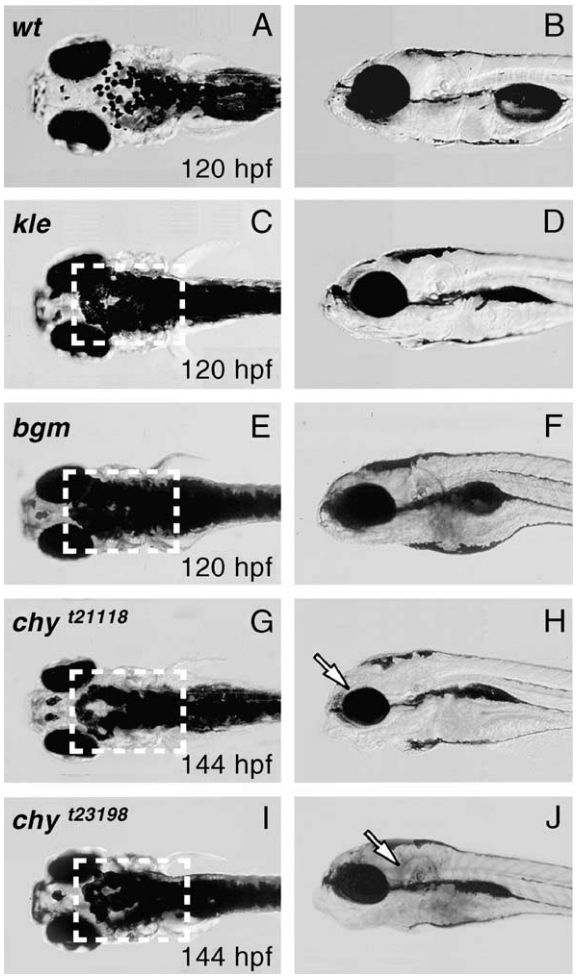

Fig. 1. External phenotypes of mutant animals. Dorsal (A, C, E, G, I) and lateral (B, D, F, H, J) views of wild-type and mutant larvae. (A) Melanophores in wild-type larvae are contracted in the dorsal regions of the head. (C, E, G, I) In contrast, melanophores in mutant larvae are abnormally dark. The head of the *kle* mutant larvae, for example, is nearly completely covered by black pigmentation (dashed box in panel C). A similar phenotype is seen in *bgm* and *chy* (dashed boxes in panels E, G, and I). (B, D, F, H, J) In a lateral view, *kle* and *bgm* animals (panels D and F, respectively) appear nearly indistinguishable from the wild type (B). The *chy* animals, on the other hand, display a reduction of eye size and brain necrosis (*t23198* allele, arrow in panel J). In all panels, anterior is right and dorsal is up.

ventrally (not shown). Overall, *kle* mutants retain the normal wild-type morphology with the exception of the swim bladder, which is absent in some mutant larvae. A phenotype similar to that of *kle* is also present in the *bgm* mutant strain (Fig. 1E). Morphologically, the *bgm* mutants appear largely normal (Figs. 1E, F). At 120 hpf, melanophores are abnormally dark on the dorsal and ventral trunk of mutant larvae (Fig. 1E, and not shown). In the third mutant strain, *chy*, the degree of melanophore defect is similar to *kle* and *bgm*. The *chy* animals display, however, additional abnormalities: the chy^{t21118} allele causes a reduction in the size of the eye cup and lens at 144 hpf (Fig. 1 arrow in H, and data not shown). The chy^{t23198} mutation, in addition to eye size reduction, produces a cloudy appearance of the brain, which suggests degeneration (Fig. 1 arrow in J). Swim bladders do not develop in the *chy* mutants, and are only occasionally present in the *bgm* homozygotes. Once pigmentation defects become obvious, the *bgm* and *chy* mutants barely respond to touch. All mutant animals die by 8 dpf.

The external defects in *kle*, *bgm*, and *chy* are not apparent during early developmental stages. Embryos from crosses between mutant heterozygotes show no apparent signs of developmental defects until 120 hpf. Prior to this stage, melanophores of all mutant strains are evenly spaced and frequently display a compact appearance, typical of wild-type embryos (data not shown, but see Fig. 1A). Likewise, during the first 96 h of development, the eye and the lens of the *chy* homozygotes do not reveal a size reduction, and the brain in the chy^{t23198} homozygotes contains no visible signs of degeneration even upon close examination.

Histological analysis of mutant phenotypes

In the wild-type retina, six major classes of neurons localize to precise positions within the three main cell layers by 60 hpf. This laminar arrangement is even more distinct by 120 hpf (Fig. 2A). To investigate whether the *kle*, *bgm*, and *chy* mutations alter the fate of retinal neurons, we inspected the appearance of mutant eyes on histological sections (Fig. 2). The most obvious abnormality in mutant retinae is the presence of empty spaces in the inner portion of the INL, most likely due to cell degeneration (arrows in Figs. 2E, H, K, and N compare to the wild type in B). In all mutant retinae examined ($n \geq 10$ for each allele) cell degeneration was confined to the inner portion of the INL. No obvious degenerative changes were observed in the ganglion cell layer and the photoreceptor cell layer at this or at later developmental stages. In *chy*, the loss of INL neurons is accompanied by a size reduction of the entire retina and the lens (Fig. 2K). Despite its smaller size, the lens differentiates largely in a normal fashion. In addition to the INL defects, the structure of the IPL is compromised in all mutants. The IPL appears less compact compared to that in the wild type, and eventually displays obvious holes in the center and periphery, indicating that cell degeneration has also affected neuronal processes.

To determine when the INL cell loss first becomes detectable, we performed histological analyses between 84 and 144 hpf in 12-h intervals. The time of phenotype onset varies somewhat among mutant alleles. While in *kle* and *bgm* mutant retinae, cell loss is first detectable by 120 hpf, in *chy* mutants cell degeneration becomes apparent by 96 hpf (arrows in Figs. 2D, G, J, and M, compare to the wild type in A). In addition to the retinal phenotype, all mutant alleles examined cause cell loss in the midline brain regions (arrows in Figs. 2F, I, L, and O, compare to the wild type in C). The onset of brain degeneration coincides with the appearance of retinal cell loss (data not shown).

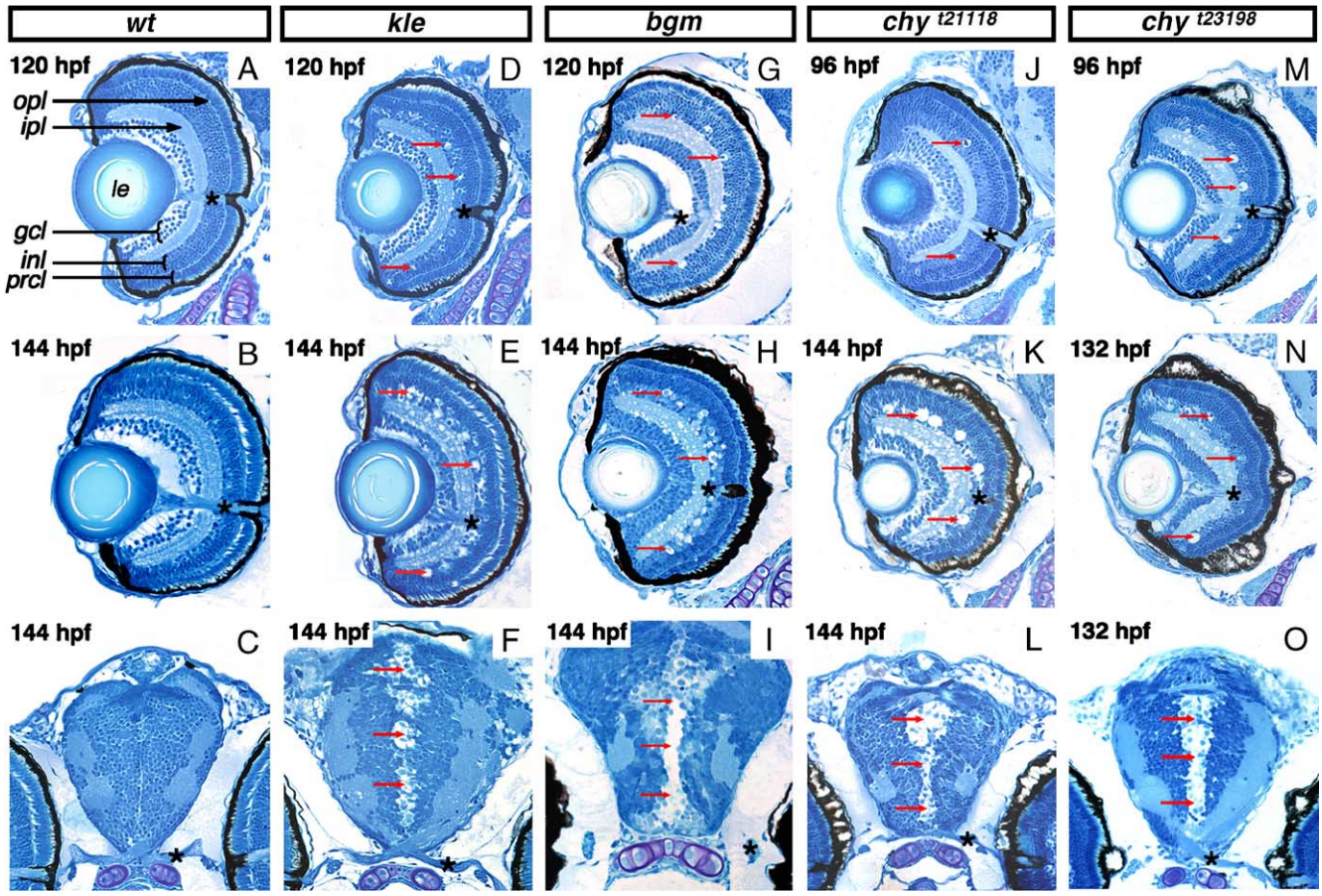

Fig. 2. Histological analysis of mutant phenotypes in the retina and brain. Transverse sections through central retinae and brains of wild-type and mutant animals at 96 to 144 hpf in the plane of the optic nerve. (A, D, G, J, M) The layered arrangement of retinal neurons is clearly visible at 96–120 hpf. (A) INL neurons in wild-type animals show uniform distribution and are densely packed. (D, G) Starting at 120 hpf, the retinae of the *kle* and *bgm* mutants display a mild cell loss in the inner portions of the INL (arrows). (J, M) In *chy* mutants, similar defects become obvious slightly earlier at 96 hpf (arrows). Two alleles of *chy*, chy^{t21118} and chy^{t23198}, produce phenotypes of somewhat different strength at 96 hpf. chy^{t23198} appears stronger (M) than chy^{t21118} (J). (B) The compact structure of the INL in the wild-type retina persists at 6 dpf. (E, H, K, N) In contrast to that, the INL of mutant retinae shows cell degeneration restricted to the inner portions of the INL, presumably the amacrine cell layer (arrows). (E–H) In *kle* (E) and *bgm* (H) mutants, cell degeneration appears restricted to the presumptive amacrine cell layer. (K, N) In *chy* mutants, this phenotype is accompanied by a decrease of eye and lens size. In addition, the IPL of mutant retinae contains small holes (E, H, K, N) which are absent in the wild type (B). (F, I, L,O) Mutant animals also experience region-specific cell degeneration in the brain. While the brain of wild-type animals appears compact (C), mutants show signs of cell loss in the midline region at ca. 132–144 hpf (arrows in panels F, I, L, and O). Asterisks indicate the optic nerve. Dorsal is up in all sections. *gcl*, ganglion cell layer; *inl*, inner nuclear layer; *prcl*, photoreceptor cell layer; *ipl*, inner plexiform layer; *opl*, outer plexiform layer; *le*, lens; hpf, hours post-fertilization.

Apoptosis in mutant retinae

To investigate the distribution of cell death in mutant animals, we performed TUNEL analysis. For each mutant strain, we inspected sections from at least 5 mutant individuals, and compared them to those obtained from at least 5 wild-type siblings. In agreement with histological data, we detect an increased number of TUNEL-positive cells in the retinae of all three mutant lines at 5 to 6 dpf. Apoptotic profiles are dramatically more frequent in the inner region of the INL of all three mutant lines, compared to their wild-type siblings (Figs. 3A–D). No significant changes are observed in the GCL, PRCL, and the outer half of the INL in *chy* and *brg* mutants (see graphs in Fig. 3). In addition to the INL defects, the *kle* mutant retinae display an elevated level of cell death in the photoreceptor cell layer (Fig. 3, graphs). As the overall histological appearance of the *kle* photoreceptor cell layer is normal at this stage (Fig. 2E), apoptosis is likely to affect only a small subset of photoreceptor cells. For reasons that we do not fully understand, photoreceptor cell death is detected predominantly in the ventral retina. Our TUNEL data indicate that cell degeneration in mutant animals is of apoptotic nature and, with one exception, is restricted to the inner portion of the INL, presumably affecting the survival of retinal amacrine cells.

Phenotypes of specific amacrine cell subpopulations

To determine the magnitude of cell loss in mutant retinae, we visualized the appearance of the entire amacrine cell layer with an antibody directed against the Hu polypeptide, which is expressed in amacrine and ganglion cells. In all

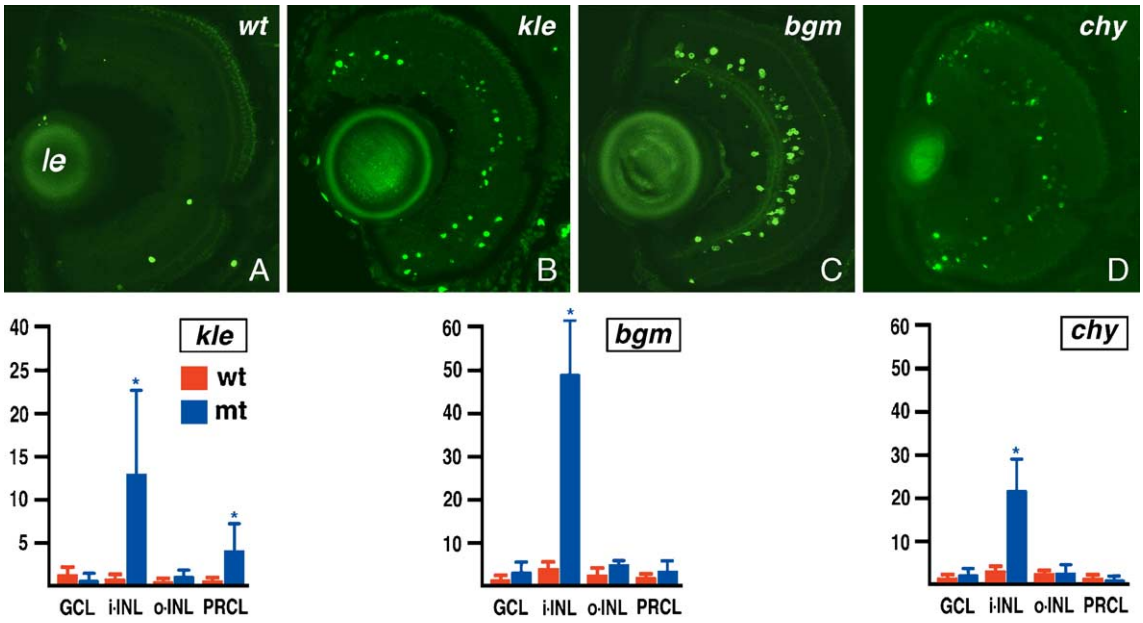

Fig. 3. Cell death in mutant retinae. To evaluate the distribution of cell death in mutant eyes, we performed TUNEL analysis at 5 dpf in *chy* and *bgm* and at 6 dpf in *kle*. (A) Wild-type individuals show little apoptotic cell death in the retina at 6 dpf. By contrast, *kle* (B), *bgm* (C), and *chy* (D) mutant eyes contain numerous apoptotic profiles located mostly in the inner INL. The counts of TUNEL-positive nuclei in individual retinal cell layers revealed that statistically significant differences are indeed observed in the inner INL, the area predominantly occupied by amacrine cells. In addition, *kle* retinae display elevated cell death in the ventral portion of the photoreceptor cell layer. Graphs provide quantitative evaluation of cell death from mutants and their wild-type siblings (at least 5 individuals were examined for each data point). Standard deviation is provided and statistically significant differences are indicated by asterisks. GCL, ganglion cell layer; i-INL, proximal inner nuclear layer; o-INL, distal inner nuclear layer; PRCL, photoreceptor cell layer; *le*, lens. In all panels dorsal is up.

mutants examined, Hu-positive amacrine cells in the INL appear somewhat disorganized and are significantly reduced in numbers (Table 2 and not shown). In contrast to amacrine cells, in *kle* and *bgm* retinae, the numbers of photoreceptor and ganglion neurons as well as Mueller glia remain unchanged. In *chy* animals, all retinal layers contain fewer cells (Table 2).

Numerous investigations of the vertebrate retina demonstrated that the amacrine cell population consists of many morphologically and biochemically distinct cell types that can be distinguished using antibodies or other staining methods. To determine whether the *kle*, *bgm*, and *chy* phenotypes uniformly affect the entire amacrine cell class, or are restricted to a subset of these cells, we performed immunohistochemical analyses with markers of amacrine cell subpopulations. Mutant animals and their wild-type siblings were fixed at 6 dpf, cryosectioned, and stained with appropriate reagents. As the mutant phenotype is sometimes difficult to distinguish on the basis of external appearance, sections were counterstained with nuclear markers, YoPro or Hoechst. This allowed us to visualize empty spaces that degenerating cells leave in mutant retinae.

A common feature of amacrine cell defects in all mutants examined is a sharp reduction of GABA-positive cells, one of the most numerous amacrine cell subpopulations (Table 2). This phenotype is observed in INL and GCL alike, but the strengths of mutant phenotypes in these two layers do not correlate with each other. The loss of GABA-positive cells is the least pronounced in *kle* (Fig. 4 and Table 2), the strongest in *chy* (Fig. 5 and Table 2), and of an intermediate strength in *bgm* (Fig. 6 and Table 2). Parvalbumin (Pv)-positive cells are another sizable subpopulation of amacrine neurons, which overlaps with GABA-immunoreactive cells by ca. 20% (data not shown). The Pv-positive population is also strongly reduced in *kle* and *chy* (Table 2). The staining of Pv-positive cells varies in intensity. In addition to brightly staining cells, some neurons display faint immunoreactivity. We have compared the frequency of faintly labeled cells in wild-type and mutant animals. For *kle* and *bgm*, the population of weakly immunoreactive cells is not affected, while in *chy*, its size is reduced only by ca. 20%, which may reflect the overall decrease of eye size in this mutant (data not shown).

Similar to Pv-positive neurons, the choline acetyltrasferase (ChAt)-immunoreactive cells are less frequent in *kle* and *chy* but are not affected in *bgm* mutants. In the rabbit retina, cholinergic amacrine cells are known to be GABA-immunoreactive (Brecha et al., 1988). The reduction of this cell population may thus be related to the loss of GABA-positive cells. In contrast to GABA-, Pv-, and ChAt-immunoreactive cells, the populations of serotonin- and tyrosine hydroxylase (TH)-positive cells are unchanged in *kle* and *bgm*, and Neuropeptide Y (NPY)-immunoreactive cells display the wild-type frequency in all mutants. These observations indicate that mutant loci compromise the survival of specific amacrine cell subpopulations.

Table 2
Cell fate analysis in mutant retinae

Major cell classes in mutant retinae of *kle*, *chy*, and *bgm*

6 dpf	Hu (INL)	Hu (GCL)	CA	Zpr1	Bipolar cell nuclei
wt (kle)	97 ± 10 (15)	82 ± 9 (11)	21 ± 6 (23)	75 ± 12 (8)	281 ± 19 (6)
kle^{t24734}	76 ± 19 (12)	91 ± 13 (12)	20 ± 6 (13)	76 ± 5 (8)	269 ± 23 (6)
Δ	22%	–	–	–	–
wt (bgm)	107 ± 13 (10)	106 ± 14 (10)	26 ± 2 (9)	92 ± 9 (14)	294 ± 25 (7)
bgm^{t21127}	73 ± 7 (9)	106 ± 12 (7)	26 ± 4 (9)	90 ± 10 (12)	262 ± 13 (6)
Δ	32%	–	–	–	11%
wt (chy)	108 ± 16 (12)	103 ± 14 (12)	23 ± 6 (12)	94 ± 7 (10)	286 ± 14 (7)
chy^{t21118}	75 ± 10 (12)	84 ± 11 (12)	17 ± 5 (13)	78 ± 7 (10)	241 ± 18 (6)
Δ	31%	18%	26%	17%	16%
wt (chy)	92 ± 11 (8)	87 ± 15 (8)	28 ± 3 (8)	90 ± 9 (8)	NA
chy^{t23198}	35 ± 11 (8)	57 ± 7 (8)	23 ± 3 (8)	76 ± 5 (8)	NA
Δ	62%	34%	18%	16%	NA

Amacrine cell subpopulations in mutant retinae

6 dpf	GABA (INL)	GABA (GCL)	Pv (INL)	Pv (GCL)	ChAt (INL)	Ser	NPY	TH
wt (kle)	68 ± 5 (11)	18 ± 4 (11)	18 ± 5 (15)	29 ± 6 (15)	13 ± 3 (11)	5 ± 2 (14)	2 ± 1 (16)	5 ± 2 (15)
kle^{t24734}	33 ± 11 (15)	12 ± 5 (15)	11 ± 6 (19)	19 ± 5 (19)	9 ± 2 (11)	6 ± 2 (14)	2 ± 1 (12)	5 ± 1 (6)
Δ	51%	33%	39%	34%	31%	–	–	–
wt (bgm)	65 ± 8 (10)	17 ± 4 (10)	16 ± 8 (12)	52 ± 5 (12)	13 ± 4 (6)	7 ± 2 (10)	2 ± 1 (9)	6 ± 3 (9)
bgm^{t21127}	25 ± 5 (7)	9 ± 4 (7)	11 ± 5 (11)	50 ± 6 (11)	12 ± 2 (5)	6 ± 2 (8)	1 ± 1 (11)	5 ± 1 (12)
Δ	62%	47%	–	–	–	–	–	–
wt (chy)	61 ± 9 (10)	15 ± 4 (10)	16 ± 8 (7)	43 ± 6 (7)	13 ± 3 (13)	5 ± 2 (15)	1 ± 1 (12)	5 ± 2 (11)
chy^{t21118}	18 ± 7 (12)	0 ± 1 (12)	2 ± 3 (8)	34 ± 5 (8)	9 ± 3 (15)	3 ± 1 (13)	1 ± 1 (17)	4 ± 2 (17)
Δ	70%	100%	88%	21%	31%	40%	–	–
wt (chy)	NA	NA	16 ± 4 (8)	32 ± 12 (8)	NA	NA	2 ± 1 (8)	4 ± 1 (8)
chy^{t23198}	NA	NA	2 ± 1 (8)	36 ± 8 (8)	NA	NA	2 ± 1 (8)	2 ± 1 (8)
Δ	NA	NA	88%	–	NA	NA	–	50%

Cell counts in mutants and their wild-type siblings of *kle*, *bgm*, and *chy* strains at 6 dpf. Each number represents an average cell count for a specific cell population evaluated on single transverse sections through retinae of wild-type and mutant animals. Standard deviation is provided, and the numbers of individuals used to calculate averages are indicated in parentheses. Each group of mutants is compared to their wild-type siblings from the same clutch of embryos. Statistical analysis was carried out using Mann–Whitney *U* test. Percentage change is provided only in cases where statistically significant differences are observed. Most counts were performed using projections of confocal *z*-series image stacks. For some cell populations, a statistically significant difference in cell counts was observed between wild-type siblings of different mutants. Changes in reagent concentrations as well as variation in fixation and antibody incubation procedures may account for this variability. Values with decimal fractions are rounded to whole numbers. NA, not analyzed.

As the inner plexiform layer is the main destination of amacrine cell processes, one would expect that amacrine cell mutants affect its organization. IPL changes are indeed observed in mutant strains. The *kle* and *bgm* phenotypes are accompanied by a decrease of the Pv immunoreactivity in the outer portion of the IPL, presumably reflecting a loss of processes that originate from Pv-positive neurons (Figs. 4 and 6C, D, inset arrows). A nearly complete loss of Pv staining in both the inner and the outer portion of the IPL is observed in *chy* (arrows in Figs. 5C and D insets). The NPY- and choline acetyltransferase-immunoreactive processes remain, however, largely unchanged in mutant animals, indicating that IPL defects are also specific to selected subpopulations of amacrine cells.

The specificity of mutant phenotypes varies. The *bgm* mutation appears to produce the most specific defect, which predominantly affects amacrine cells. The *chy* defect, on the other hand, is the least specific and produces a reduction in cell number of roughly 20–30% in all major cell classes examined, including photoreceptor cells and Mueller glia. As cell degeneration is not obvious outside the inner portion of the INL in the *chy* retinae, this observation indicates that the *chy* locus may play a dual role in retinal differentiation. First, it may function in the determination of the overall retinal size, and second it may be necessary for the differentiation of selected retinal cell classes.

Early onset of amacrine cell defects

As indicated by birthdating studies, neurogenesis in the zebrafish retina starts at approximately 28 hpf in the ganglion cell layer. The first amacrine cells are born 10 h later, at ca. 38 hpf, and gradually differentiate over 30 h or so (Hu and Easter, 1999; Schmitt and Dowling, 1999). By 72 hpf, many amacrine cell-specific markers are detectable in wild-type retinae. To investigate whether amacrine cell loss at 5 dpf is due to cell-fate changes at earlier stages of embryogenesis, we inspected mutant retinae at ca. 80 hpf. At this stage, mutant animals cannot be recognized on the basis of their external appearance or via histological analysis of their retinae on plastic sections. To identify mutant eyes at 80 hpf, we surgically removed one eye from each embryo at about 75–

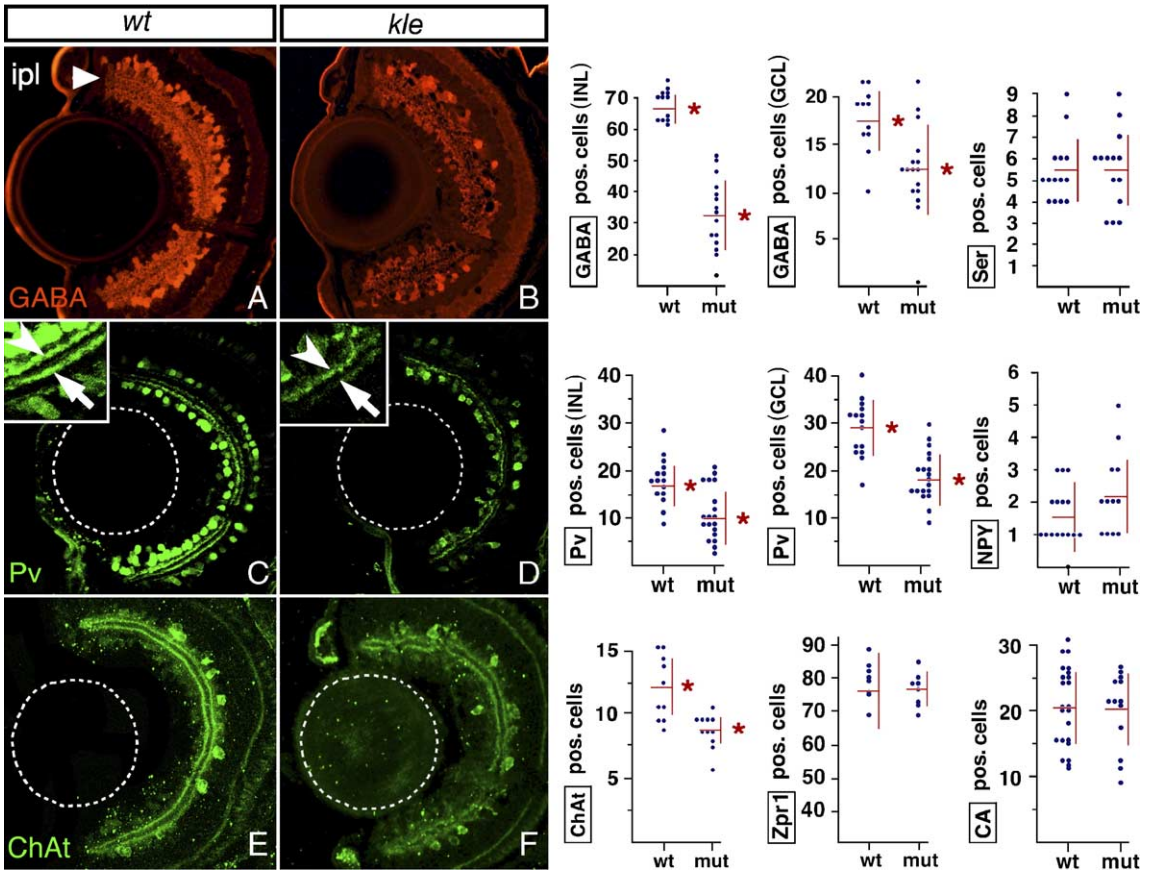

Fig. 4. Selected subpopulations of amacrine cells degenerate in *kle*. Analysis of the *kle* mutants and their wild-type siblings with markers of specific retinal cell populations at 6 dpf. (A, B) A strong reduction of GABA-immunoreactive cell number is obvious in mutants (B) compared to their wild-type siblings (A). To assure that all GABA-positive cells in mutant retinae were taken into account, the fluorescence in panel B is slightly enhanced compared to panel A. (C, D) A significant size reduction is also detected for Pv-positive cell populations in the mutant GCL and the INL (D), when compared to the wild type (C). Processes of Pv-positive amacrine neurons are present in the inner (C, inset, arrowhead) and the outer (C, inset, arrow) sublaminae of the wild-type IPL. In contrast to that, the outer layer of Pv-positive processes is much less prominent in mutant retinae (D, inset, arrow), while the inner layer retains prominent staining (D, inset, arrowhead). (E, F) ChAt-positive cells are less frequent in the mutant retina (F) when compared to the wild type (E). Graphs on the right-hand side provide a comparison of cell counts in the retinae of mutant and wild-type siblings. Each dot represents the number of cells in a separate retina. Red horizontal and vertical lines in each graph indicate the average and the standard deviation, respectively. For Pv staining, only intensely labeled cells were taken into account. Asterisks indicate changes of statistical significance as evaluated by the Mann–Whitney *U* test. GCL, ganglion cell layer; INL, inner nuclear layer; ipl, inner plexiform layer. CA, ChAt, GABA, NPY, Pv, and Ser stand for carbonic anhydrase, choline acetyltransferase, gamma-aminobutyric acid, neuropeptide Y, parvalbumin, and serotonin, respectively. In panels A–D, dorsal is up, lens is left.

80 hpf and fixed it for immunohistochemical analysis. Approximately 3 days after the surgery, eye donor animals were fixed, and analyzed on plastic sections to determine their genotype. Once mutant larvae were identified using this method, the eyes collected earlier were processed for immunohistochemistry using anti-GABA and anti-Pv antibodies. In parallel to these amacrine cell markers, retinae were stained with the Zpr1 antibody or Hoechst nuclear stain to evaluate photoreceptor cell layer morphology as an independent control for staging. Retinae that did not contain a prominent Zpr1 expression or elongated photoreceptor cells throughout the entire PRCL were considered delayed and eliminated from the analysis.

In *chy*^{t21118} mutants, we have not detected a significant difference in the numbers of GABA- and Pv-positive cells, compared to their wild-type siblings (Fig. 7). In contrast to that, the retinae of *kle* animals display a decrease in the number of GABA-positive amacrine cells in the INL at 80 hpf (Figs. 7A and B). While wild-type retinae contain the average of 58 GABA-positive cells, on average, 49 cells are present in the eyes of *kle* mutant homozygotes ($n \geq 13$ sections from retinae of at least 4 individuals), representing a decrease of ca. 15% ($P < 0.05$). A statistically significant decrease was not seen in other cell populations of *kle* homozygotes: Pv-positive amacrine cells and photoreceptors (Fig. 7). These results suggest that the *kle* defect is present shortly after the formation of a functional retina, and raise the possibility that other amacrine cell defects observed in *kle* may develop as a secondary consequence of the GABA deficiency.

Retinae of kle and chy animals are functionally defective

Although amacrine cells display the most severe differentiation defects in all mutant strains investigated and other

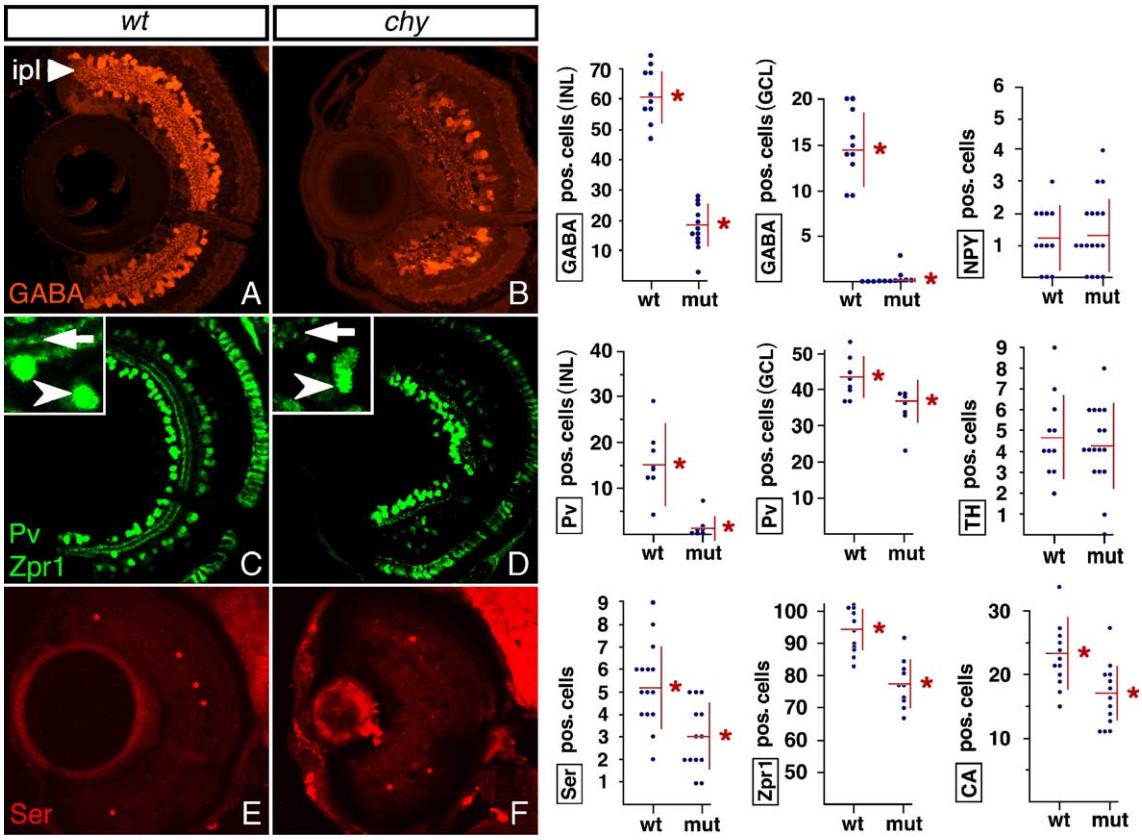

Fig. 5. Mutations of the *chy*^{t21118} locus produce a loss of selected amacrine cell subpopulations. Analysis of the *chy* mutants and their wild-type siblings with markers of specific retinal cell populations at 6 dpf. (A, B) A reduction of GABA-immunoreactive cell number is obvious in the *chy* mutants (B) in comparison to their wild-type siblings (A). (C, D) The mutant INL contains fewer Pv-positive cells (D) compared to wild-type animals (C). The remaining Pv-positive cells in the mutant INL show somewhat elongated morphology (D, inset, arrowhead), different from the one observed in the wild type (C, inset, arrowhead). In contrast to the wild type (C, inset, arrow), the processes of Pv-positive cells are barely detectable in the IPL of mutant retinae (D, inset, arrow). (E, F) The frequency of serotonin-positive amacrine cells displays a ca. 40% decrease in a mutant retina (F) when compared to the wild type (E). Graphs on the right-hand side provide a comparison of cell counts in the retinae of mutant and wild-type siblings. Each dot represents the number of cells in a separate retina. Red horizontal and vertical lines in each graph indicate the average and the standard deviation, respectively. For Pv staining, only intensely labeled cells were taken into account. Asterisks indicate changes of statistical significance as evaluated by the Mann–Whitney *U* test. GCL, ganglion cell layer; INL, inner nuclear layer; ipl, inner plexiform layer. CA, GABA, NPY, Pv, Ser, and TH stand for carbonic anhydrase, gamma-aminobutyric acid, neuropeptide Y, parvalbumin, serotonin, and tyrosine hydroxylase, respectively. In panels A–F, dorsal is up, lens is left.

cell classes appear either morphologically intact or are affected to a lesser degree, it remains possible that functional defects are also present outside the INL, in photoreceptor cells for example. In addition, one would like to know how amacrine cell loss affects retinal function. The electrical activity of inner and outer nuclear layers in the retina can be evaluated using electroretinography (ERG). Zebrafish ERG responses are well documented and similar to other vertebrate species consist of at least three components: a-, b-, and d-waves (reviewed in Seeliger et al., 2002). The corneal negative a-wave reflects the function of the outer retina and is quickly obscured by the large positive b- and d-waves, which reflect the activity of the inner nuclear layer. To evaluate whether ERG responses are affected in mutant retinae, we performed recordings from isolated larval eyes at 6 dpf. Light stimulation of wild-type retinae produces robust responses over a range of light intensity that varies by four orders of magnitude (Fig. 8A). Unexpectedly, most *chy* mutant individuals do not respond to light at any level of intensity at 6 dpf (6 out of 11 individuals tested) while the remaining ones exhibit very small b-waves when compared to the responses of wild-type siblings (Figs. 8B and C, compare to the wild type in A). This result indicates that *chy* mutants exhibit a defect of photoreceptor layer function. To see whether this defect is present prior to the appearance of cell loss in mutant retinae, we assayed ERG responses in *chy* mutants at 4 dpf using the same light exposure regimen. Since the mutant phenotype is not distinguishable at this stage, we applied the same eye dissection strategy as described for immunostaining experiments above. We found that, indeed, the *chy* mutant animals display an abnormal ERG response already at 4 dpf (Fig. 8G, compare to wild-type siblings in F). The majority of mutants tested exhibit a sharply reduced b-wave response (5 out of 8 individuals tested) and the remaining ones fail to produce any response at all (Fig. 8H). These results indicate that, in addition to amacrine cell defects, the *chy*^{t21118} allele produces an early loss of photoreceptor function. To assess

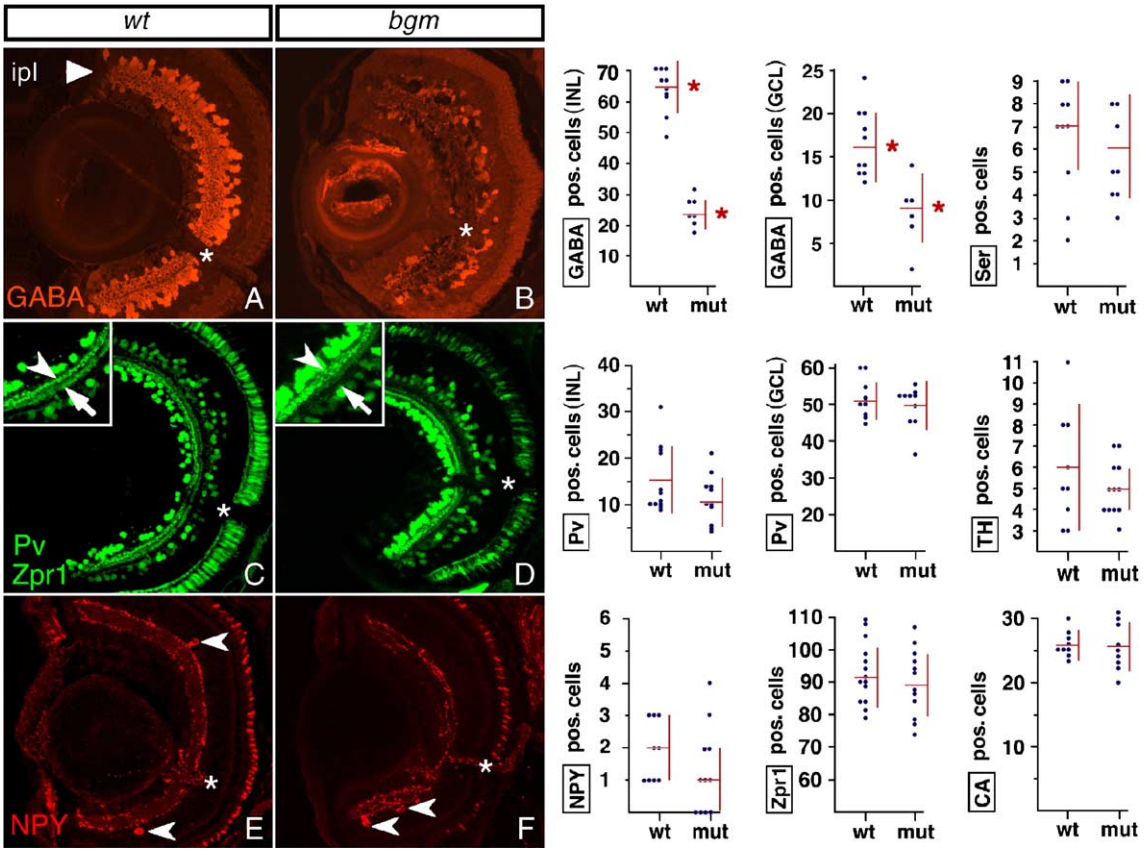

Fig. 6. Selected subpopulations of amacrine cells degenerate in *bgm*. Analysis of the *bgm* mutants and their wild-type siblings with markers of specific retinal cell populations at 6 dpf. (A, B) A sharp reduction is seen in the population of GABA-positive cells in mutant retinae (B), compared to the wild type (A). GABA-positive processes are not apparent in the mutant IPL, compared to wild-type sibling animals of the same age (arrowhead in panel A). (C, D) The number of Pv-positive cells in the mutant INL appears reduced (D), compared to wild-type individuals (C). This difference, however, is not statistically significant (graph). The Pv-positive neuronal processes are either reduced or absent in the outer (arrows) but not the inner (arrowheads) IPL. Other populations of amacrine cells, including neuropeptide Y-positive neurons (arrowheads in panels E and F), do not show a significant reduction. Similarly, the number Mueller glia and photoreceptors cells remain unchanged between wild-type and mutants (graphs). Graphs on the right-hand side provide a comparison of cell counts in the retinae of phenotypically mutant and wild-type siblings. Each dot represents the number of cells in a separate retina. Red horizontal and vertical lines in each graph indicate the average and the standard deviation, respectively. For Pv staining, only intensely labeled cells were taken into account. Asterisks indicate changes of statistical significance as evaluated by the Mann–Whitney *U* test. GCL, ganglion cell layer; INL, inner nuclear layer; ipl, inner plexiform layer. CA, GABA, NPY, Pv, Ser, and TH stand for carbonic anhydrase, gamma-aminobutyric acid, neuropeptide Y, parvalbumin, serotonin, and tyrosine hydroxylase, respectively. In panels A–F, dorsal is up, lens is left.

whether this photoreceptor defect is associated with structural abnormalities, we performed electron microscopic analysis of mutant photoreceptor cells. No obvious differences are found in the appearance of outer segments, inner segments, synaptic termini, or cell junctions of *chy* photoreceptors (Fig. 8E, and data not shown).

In contrast to *chy*, the *kle* mutation mainly affects the INL function. *kle* mutant animals display a ca. two-fold decrease of the b-wave amplitude, compared to their wild-type siblings at the same levels of light intensity (Fig. 8D, quantitated in J). In contrast to the b-wave, the a-wave appears unaffected. To evaluate the photoreceptor response more precisely, we isolated the a-wave by inhibiting INL function by pharmacological means (Kainz et al., 2003; Wong, 2005). At low light intensity levels, the *kle*−/− a-wave amplitude (n = 4) is nearly identical to that of wild-type siblings (n = 5). The differences at higher light intensity, although observed, are not statistically significant (Fig. 8I). These results indicate that the *kle* mutation does not significantly affect the photoreceptor cell layer functions. Thus, the decrease of the *kle* b-wave amplitude is unlikely to originate in the photoreceptor cell layer and most probably reflects an INL malfunction, possibly due to amacrine cell loss.

chy function is cell-nonautonomous in the amacrine cell layer

The regular spacing of amacrine cell perikarya in the plane of the inner nuclear layer and the precise ratios of different cell types suggest that cell–cell interactions play a role in the differentiation of amacrine neurons. One would therefore expect that a defect in one amacrine cell subpopulation may be followed by secondary, cell-non-

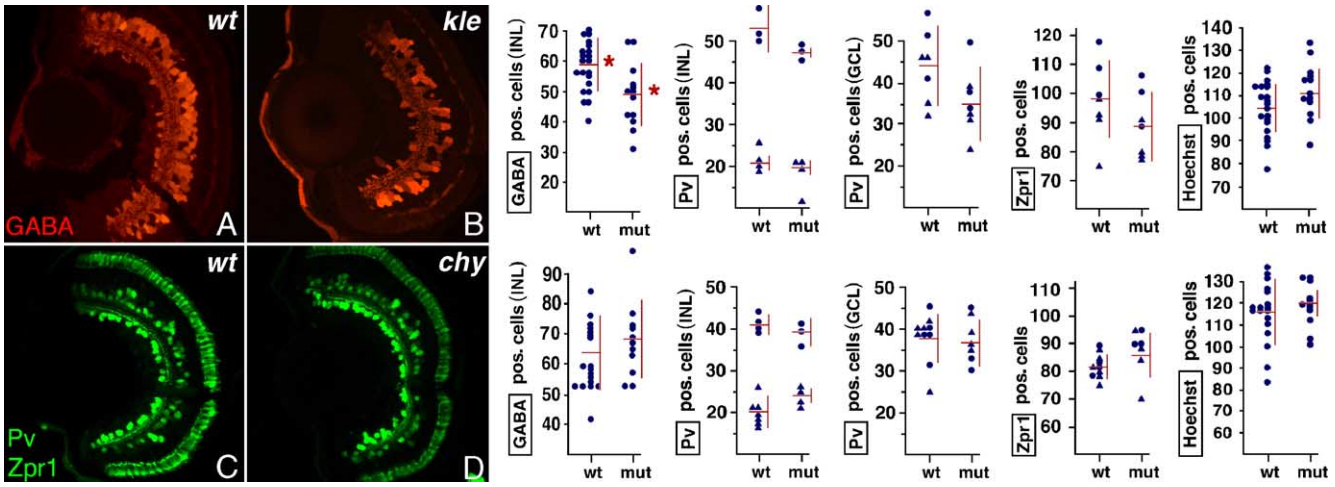

Fig. 7. The immunostaining of wild-type and mutant retinae at approximately 80 hpf. (A, B) In *kle* mutants (B), GABA-immunoreactive amacrine cells in the INL are less frequent than in their wild-type siblings (A). (C, D) No significant difference in the Pv-positive amacrine cell population is observed between *chy*^{t21118} mutant embryos (D) and their wild-type siblings (C). Counts of Zpr1-positive cells and Hoechst stained nuclei were performed in the photoreceptor cell layer to provide an estimate of photoreceptor layer differentiation. Except for the GABA and Hoechst counts in *kle* and *chy* retinae, each dot (triangle) represents the number of cells in a separate retina. Results from two independent experiments are indicated with dots and triangles, respectively. Differences in cell counts in these two experiments are most likely due to the fact that even a small age difference involves pronounced changes of cell number at early stages of amacrine cell layer differentiation. GABA and Hoechst analysis was performed on sections from retinae of 4 individuals. Graphs on the right-hand side provide a comparison of cell counts in the retinae of mutant and wild-type siblings. Asterisks indicate changes of statistical significance while red horizontal and vertical lines in each graph indicate the average and the standard deviation, respectively. Statistical analysis was carried out using Mann–Whitney *U* test for GABA and Hoechst staining results in *kle* animals. The remaining data were evaluated using Student's *t* test. For Pv staining, only intensely labeled cells were taken into account. GABA and Pv stand for gamma-aminobutyric acid and parvalbumin, respectively. In panels A–D, dorsal is up, lens is left.

autonomous phenotypes in other cells. To test whether this is the case in zebrafish mutants, we performed mosaic analysis of the *chy* mutant phenotype. Pv-positive cells in the INL are one of the most severely affected cell populations in mutant retinae. We decided to investigate whether the loss of these cells is due to an intrinsic defect in this cell population or it is caused by an abnormal environmental factor, such as a deficit in a cell population which interacts with Pv-positive cells. In zebrafish, this question can be addressed by generating mosaic animals via blastomere transplantation between genetically divergent host and donor embryos. We generated two classes of genetically mosaic animals: embryos containing small clones of donor-derived mutant cells in otherwise wild-type host retinae, and embryos containing small clones of wild-type donor-derived cells in otherwise mutant host retinae. Animals containing clones of wild-type cells in wild-type retinae, or clones of mutant cells in mutant retinae served as controls. Host and donor genotypes were determined on the basis of external phenotype at 6 dpf. These studies revealed that the frequency of Pv-positive amacrine cells in donor-derived clones depends on the genotype of host rather than donor retinae (Fig. 9). Mutant cells in the environment of wild-type retinae contribute to the Pv-positive cell population with the same frequency as wild-type cells. Consistent with this result, wild-type cells in the environment of mutant retinae contribute to the Pv-positive cell population with the same frequency as mutant cells in mutant environment (Fig. 9B). As expected, the frequencies of photoreceptor cells do not display statistically significant differences in all four groups of blastomere transplantation embryos (Fig. 9 table). These observations indicate that the loss of Pv-positive amacrine cells in *chy* is a secondary consequence of an environmental deficiency, most likely in another retinal cell class.

Pv-positive neurons constitute a small subset of amacrine cells. Thus, the loss of Pv-positive cells may be a consequence of a defect in another amacrine cell subpopulation. It is thus possible that while the Pv-cell phenotype is cell-nonautonomous, the phenotypes of other amacrine cell populations are autonomous. To test whether this is the case, we performed mosaic analysis of the mutant phenotype in GABA-positive cells. GABA-immunoreactive cell population is severely depleted in *chy* mutant animals by 6 dpf. We investigated whether this reduction is due to an intrinsic defect in GABA-positive cells, or due to a deficiency in the environment of these neurons. Mosaic analysis revealed that the frequency of donor-derived GABA-positive mutant cells is not significantly improved in wild-type environment. Consistent with this result, the frequency of donor-derived wild-type cells is not significantly different in mutant environment, compared to wild-type retinae (Fig. 9). The results of mosaic analysis indicate that, in contrast to Pv-positive cells, the phenotype of GABA-positive neurons in *chy* retinae does not display a significant nonautonomy.

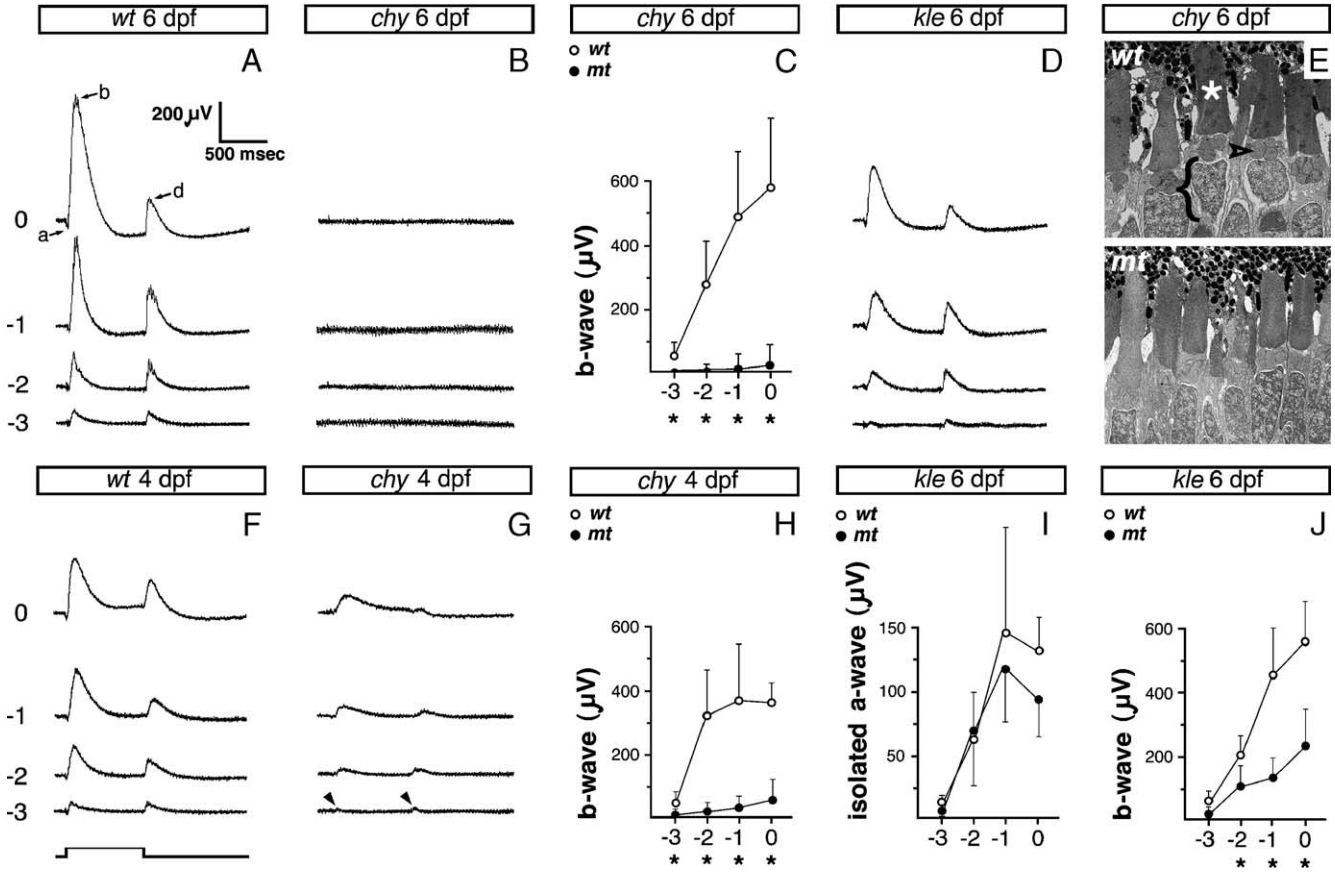

Fig. 8. Representative ERG responses from *kle*^{t24734} and *chy*^{t21118} animals. All responses were elicited using 800 ms flashes and recorded at 4 levels of light intensity. (A) Prominent ERG waveforms are evident in wild-type larvae at 6 dpf and consist of a-, b-, and d-components. (B) *chy* mutant individuals almost completely lack all components of the wild-type ERG response at 6 dpf (6 out of 11 individuals tested showed no response). (C) Quantification of b-wave amplitude in *chy* mutants ($n = 11$) in comparison to the wild-type siblings ($n = 10$) shows a dramatic decrease of the b-waves amplitude at all thresholds of light intensity. (D) In *kle* mutants ($n = 5$), all components of ERG responses are present as compared to the wild-type sibling animal ($n = 4$, not shown). b-wave amplitudes, however, appear reduced in mutant individuals at all light intensities tested. (E) Electron micrographs of sections through wild-type (upper) and *chy* mutant (lower) photoreceptor cell layer at 6 dpf. No differences in photoreceptor ultrastructure are obvious between wild-type and mutant animals. (F, G) Responses of a wild-type larva at 4 dpf (F) are compared to these of the *chy* mutant sibling of same age (G). In the *chy* mutant, ERG responses are sharply reduced so that the b- and d-waves are barely detectable at low light intensity level (arrowheads). (H) Quantification of b-wave amplitudes shows a significant decrease in mutants ($n = 8$) when compared to their wild-type siblings ($n = 4$) at 4 dpf (Student's t test, $P < 0.05$). (I) Isolated a-wave amplitudes are compared between wild-type ($n = 5$) and mutant ($n = 4$) *kle* individuals at 6 dpf. Although the mutant amplitudes are somewhat reduced, the changes are not statistically significant (Student's t test, $P > 0.05$). (J) By contrast, b-wave amplitudes are significantly different between mutant ($n = 5$) and wild-type sibling ($n = 4$) individuals (Student's t test, $P < 0.05$). In panels A and F, numbers to the left indicate light attenuation in exponential units. In panels C and H–J, asterisks indicate statistical significance and vertical lines provide standard deviations.

The expression of several potential regulators of amacrine cell survival is not altered in kle, bgm, and chy retinae

Several genes, including BDNF, its receptor TrkB, as well as IGFI and II, are thought to influence amacrine cell survival (Cusato et al., 2002; Politi et al., 2001; Rickman and Rickman, 1996). An altered expression level of one or more of these factors could be the cause of amacrine cell defects in *kle*, *chy*, and *bgm* mutants. To test this possibility, we performed a semi-quantitative RT-PCR analysis of expression levels for zebrafish *bdnf*, neurotrophin receptors *ntrk2a* (formerly *trkB1*) and *ntrk3a* (*trkC1*), as well as *igf1* and *igf2* genes. The expression of all five of these loci has been previously detected in larval zebrafish eyes (Martin et al., 1995; Maures et al., 2002). Our studies revealed no differences in mRNA expression levels between mutant animals and their wild-type siblings (data not shown). In parallel, we used anti-BDNF, anti-TrkB, and anti-TrkC antibodies to evaluate expression on the protein level. These antibodies have been previously reported to recognize single bands on Western blots of zebrafish homogenates (Germana et al., 2004). Staining of wild-type retinae at 3, 5, 7, and 10 dpf revealed strong *ntrk2* expression in the optic nerve and a weakly elevated signal in the IPL. A weak *bdnf* signal was detected both in the GCL and the inner portion of the INL starting at 5 dpf. No *ntrk3* expression was found at 3 or 5 dpf. The specificity of these expression patterns was tested by peptide blocking. Both Bdnf and Ntrk2 staining were eliminated following incubation with peptides used for the production of relevant antibodies. Consistent

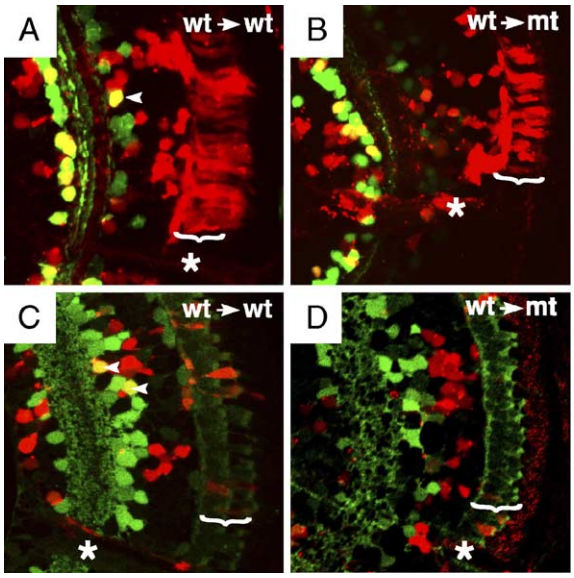

Group	Pv %	PR%	*m*	*n*
wt➔wt	2.18*	21.9	3202	75
mt➔wt	1.85*	22.8	3122	79
wt➔mt	0.48*	22.4	1682	41
mt➔mt	0.52*	24.1	576	17

Group	GABA %	PR%	*m*	*n*
wt➔wt	8.09	22.3	1706	63
mt➔wt	6.00	19.4	651	28
wt➔mt	5.86	20.9	631	26
mt➔mt	4.82	22.9	353	21

Fig. 9. Mosaic analysis of the amacrine cell survival phenotype in the INL of *chy* animals. In panels A and B, parvalbumin-positive cells are stained green. In panels C and D, GABA-positive cells are stained green. In all image panels, donor-derived cells are labeled red, and donor-derived parvalbumin- and GABA-positive cells appear yellow. (A) Clones of donor-derived wild-type cells contribute parvalbumin-positive neurons (arrowhead). (B) In the environment of mutant retinae, wild-type clones contribute much less frequently to the parvalbumin-positive cell population in the INL. (C) Clones of donor-derived wild-type cells contribute GABA-positive amacrine neurons. (D) In the mutant environment, wild-type cells contribute to the population of GABA-positive cells with a comparable frequency. Tables to the right show the frequency of donor cell contribution to parvalbumin- and GABA-positive cell populations (Pv% and GABA%, respectively), in four types of transplantation experiments. For the Pv-positive cells, this frequency depends on the genotype of host animals, indicating cell-nonautonomy. Neither host nor donor genotypes affect the frequency of donor-derived photoreceptor cells (PR%). *m* indicates the total number of cells counted in *n* clones of donor-derived cells. Asterisks indicate statistically significant differences as analyzed by the chi-square test. In all image panels, brackets indicate the photoreceptor cell layer and asterisks indicate the optic nerve, lens is right and dorsal is up.

with RT-PCR results, we did not detect any obvious differences in Bdnf and Ntrk2 staining between wild-type animals and their mutant siblings (data not shown). These data indicate that amacrine cell loss in mutant retinae is not due to the absence of expression or a gross misexpression of the genes tested. Genetic mapping will be necessary, however, to conclusively exclude the possibility the mutations in these genes are the cause of *kle*, *chy*, or *bgm* mutant phenotypes.

Discussion

The identification of mutants with impaired vision can be achieved in zebrafish using morphological criteria, the staining of specific cell populations with histochemical procedures, or behavioral tests (Baier et al., 1996; Malicki et al., 1996; Neuhauss et al., 1999). In a large-scale genetic screen, staining or behavioral assays become prohibitively labor-intensive, and frequently are not practical. A drawback of morphological screens, on the other hand, is that only obvious eye defects are isolated, while many more subtle abnormalities remain unnoticed. To identify more subtle defects, in addition to morphological criteria, we took advantage of the observation that visual system defects are frequently associated with the lack of background adaptation in zebrafish larvae. Teleost melanophores are known to redistribute their pigment granules in a microtubule-dependant fashion (McNiven and Porter, 1986; Murphy and Tilney, 1974). This behavior is known to be affected by the level of illumination (reviewed in Fujii, 2000), and appears to be disrupted in several zebrafish retinal mutants, including *lakritz* (*lak*), *brudas* (*bru*), and *out of sight* (*out*) (Malicki et al., 1996; Neuhauss et al., 1999). By searching for the lack of pigment adaptation, we identified visual system mutations that either do not cause defects in the external eye morphology or produce only subtle morphological phenotypes. Histological analysis of retinae from these animals confirmed that despite their normal external appearance, many display severe abnormalities. In this work, we focus on loci that cause cell loss in the INL: in four mutant lines that are the subject of this study, cells degenerate predominantly in the inner portion of the INL. Based on the evaluation of individual cell populations, we conclude that these mutations produce the most severe defects in amacrine neurons, while photoreceptor, bipolar, and ganglion cell layers remain unaffected or display milder abnormalities, even at advanced stages of development. Mutations in only one of the three loci examined, *chy*, cause a noticeable decrease in eye size, associated with reduced numbers of all major retinal cell classes. Even in the *chy* mutants, however, on histological sections and in TUNEL assays, cell degeneration is obvious only in the amacrine cell layer. In addition to abnormally pigmented melanophores and eye

size reduction, few other external abnormalities are recognizable in mutant animals. Histological analysis reveals, however, cell degeneration around the brain ventricle, suggesting that the mutant genes function both in the retina and in the brain.

Apoptotic cell death in mutant retinae is restricted to the proximal INL, as evidenced by TUNEL assay. The sole exception to this pattern is the photoreceptor cell layer of *kle* mutant animals. Despite the loss of some cells, however, photoreceptor function appears unchanged in *kle* ERG studies. This may be because apoptosis affects only a small subset of photoreceptor cells and is mostly confined to the ventral retina. In the proximal INL, cell death affects amacrine cells, a neuronal population that consists of many morphologically and biochemically distinct cell types. To better understand the specificity of mutant phenotypes in the amacrine cell layer, we performed immunohistochemical studies using markers of amacrine cell subpopulations. This analysis revealed that some subpopulations of amacrine neurons are selectively affected in *kle*, *chy*, and *bgm* mutant animals. A common feature of mutant phenotypes is that all of them involve a sharp decrease in the numbers of GABA-positive cells. Other populations of cells that are strongly affected, albeit less consistently, are Pv- and ChAt-positive neurons. Defects in other cell classes are even less frequent or absent. Among the three loci, the mutation of *bgm* produces the most specific phenotype in the amacrine cell layer, affecting GABA-positive cells only. Mutations in the *chy* locus, on the other hand, produce the broadest spectrum of defects. We have not observed an ectopic accumulation of any retinal cell population, indicating that the mutant loci are unlikely to play a role in the formation of gross retinal architecture. In addition to retinal phenotypes, mutant animals display similar brain defects. Overall, the similarities of mutant phenotypes suggest that all three loci may function in the same genetic pathway.

The analysis of mutant phenotypes revealed that they affect multiple cell subpopulations in the amacrine cell layer. As some of the markers that we used in our studies label overlapping cell populations, it is possible that a mutation primarily affects a single cell subpopulation characterized by a particular histochemical marker expression while defects in populations characterized by other markers merely reflect expression overlap. This could be the case, for example, for the populations of Pv- and GABA-positive cells. The loss of Pv-positive cells could result from a defect that is present in GABA-immunoreactive cells. If this was the case, only these Pv-positive cells that also express GABA would be affected. To test this possibility, we labeled wild-type retina with antibodies against Pv and GABA and found that only about 20% of Pv-positive cells in the INL are GABA-immunoreactive (data not shown). In the *kle* mutant retina, however, over 50% of Pv-positive cells are absent. These observations indicate that the loss of Pv-positive cells is not a cell-autonomous consequence of a defect in GABA expressing cells. This result, however, does not exclude the possibility that the loss of Pv cells is a cell-nonautonomous consequence of a defect in GABA-positive neurons. Amacrine cell types in the retina form synaptic connections with each other (Famiglietti, 1991; Mariani and Hersh, 1988; Yamada et al., 2003). In the absence of normal synaptic partners, some populations of amacrine cells may undergo apoptosis. Such a mechanism could lead to a nonautonomous cell loss. The relationships between the defects of different amacrine cell subpopulations in *kle*, *chy*, and *bgm* is an interesting topic that deserves investigation. Further studies of this subject in zebrafish mutants may reveal inductive, trophic, or functional interactions between different types of amacrine neurons.

Contrary to what histological analysis suggests, ERG studies of *chy* reveal a functional defect in the photoreceptor cell layer. What is the relationship between photoreceptor cell defect and amacrine cell loss in *chy* mutant retinae? A causal relationship between the loss of photoreceptor function and amacrine cell degeneration is unlikely. The strongest argument against such a possibility is the observation that although several zebrafish mutants, *elipsa* and *oval* for example, display a complete absence of ERG response, their INL neurons do not exhibit any signs of degeneration (Bahadori et al., 2003; Doerre and Malicki, 2002). Similarly, a loss of INL cells has not been observed in zebrafish photoreceptor mutants that produce milder ERG response defects (Allwardt et al., 2001; Kainz et al., 2003). The most obvious alternative possibility is that the *chy* gene plays a dual role in the retina and functions in two independent mechanisms, one required for photoreceptor function and one for amacrine cell survival.

The role of the *chy* locus in the amacrine cell layer appears even more complex in the light of mosaic analysis. The loss of Pv-positive cells in the INL is clearly nonautonomous and may originate in another amacrine cell subpopulation, or alternatively, it may originate in another retinal cell class. In contrast to Pv-positive neurons, the phenotype of GABA-positive cells does not display a significant cell-nonautonomy. Wild-type clones in mutant retinae do not contain a significantly different fraction of GABA-immunoreactive cells as compared to control mutant clones in mutant retinae. One possible interpretation of the difference between the phenotypes of Pv- and GABA-positive cells is that the nonautonomy of cell loss in Pv-positive cell population is secondary to a cell autonomous defect in GABA-positive cells. The differentiation of the amacrine cell layer and its remarkable diversity of cell types is likely to involve complex cell–cell interactions, which remain poorly understood. Mosaic analysis of the *chy* phenotype offers some of the first insights into this area.

The zebrafish mutants described in this work define a new class of retinal defects. In contrast to photoreceptor cell mutants, which have been characterized in the retinae of

numerous vertebrate species, including humans, rodents, dogs, birds, and fish (Doerre and Malicki, 2002; Dryja et al., 1990; Kijas et al., 2002; Semple-Rowland et al., 1998), genetic defects that predominantly produce severe amacrine cell loss to our knowledge have not been described in vertebrates so far. A possible exception to this state of affairs, is the *nervous* (*nr*) mutant mouse retina, characterized by a late-onset thinning of the INL and a reduced density of glycine- and GABA-positive amacrine cells (Ren et al., 2001). These two cell populations are reduced by ca. 25% in the *nr* mutant retina, a relatively weak phenotype, compared to the zebrafish amacrine cell defects described here. It is not clear whether other amacrine cell subpopulations are also affected in *nr* animals. The *nr* mouse also displays photoreceptor degeneration (White et al., 1993). Even more subtle changes of GABA expression have been suggested in the *spastic* (*spa*) mouse (Yazulla et al., 1997). Given the limited number of amacrine cell mutants characterized so far, defects in the zebrafish *kle*, *chy*, and *bgm* loci provide a unique opportunity to study the mechanisms of amacrine cell differentiation and survival in the vertebrate retina.

Acknowledgments

The authors thank Dr. Clint Makino for comments on an earlier version of the manuscript, Jens Hooge for technical assistance with sectioning zebrafish larvae during the large-scale ENU mutagenesis screen, Dr. Ed Mroz for advice regarding statistical analysis, and Norm Michaud for help with electron and confocal microscopy. Jeff Seamans was indispensable for organizing the timely delivery of reagents, while Andria Schibler and Mateo Nenadovic provided assistance with setting up crosses and collecting embryos. Dr. Michael Sandberg, Basil Pawlyk, and members of the John Dowling, as well as Stefan Neuhauss laboratories provided helpful suggestions regarding electroretinography. The anti-carbonic anhydrase antibody was provided by Dr. Paul Linser. Studies presented in this publication were supported by grants from the National Eye Institute (to JM) and the Glaucoma Foundation (to JM) and the Dept. of Ophthalmology core grant for Vision Research, P30EY14104. RD was supported by a Long-term Fellowship from the European Molecular Biology Organisation (EMBO) and the Max-Planck-Society.

References

Allwardt, B.A., Lall, A.B., Brockerhoff, S.E., Dowling, J.E., 2001. Synapse formation is arrested in retinal photoreceptors of the zebrafish nrc mutant. J. Neurosci. 21, 2330–2342.

Avanesov, A., Malicki, J., 2004. Approaches to study neurogenesis in the zebrafish retina. Methods Cell Biol. 76, 333–384.

Bahadori, R., Huber, M., Rinner, O., Seeliger, M.W., Geiger-Rudolph, S., Geisler, R., Neuhauss, S.C., 2003. Retinal function and morphology in two zebrafish models of oculo-renal syndromes. Eur. J. Neurosci. 18, 1377–1386.

Baier, H., Klostermann, S., Trowe, T., Karlstrom, R.O., Nusslein-Volhard, C., Bonhoeffer, F., 1996. Genetic dissection of the retinotectal projection. Development 123, 415–425.

Brecha, N., Johnson, D., Peichl, L., Wassle, H., 1988. Cholinergic amacrine cells of the rabbit retina contain glutamate decarboxylase and gamma-aminobutyrate immunoreactivity. Proc. Natl. Acad. Sci. U. S. A. 85, 6187–6191.

Cameron, D.A., Carney, L.H., 2000. Cell mosaic patterns in the native and regenerated inner retina of zebrafish: implications for retinal assembly. J. Comp. Neurol. 416, 356–367.

Cusato, K., Bosco, A., Linden, R., Reese, B.E., 2002. Cell death in the inner nuclear layer of the retina is modulated by BDNF. Brain Res. Dev. Brain Res. 139, 325–330.

Dmitriev, A.V., Mangel, S.C., 2000. A circadian clock regulates the pH of the fish retina. J. Physiol. 522 (Pt. 1), 77–82.

Doerre, G., Malicki, J., 2001. A mutation of early photoreceptor development, *mikre oko*, reveals cell–cell interactions involved in the survival and differentiation of zebrafish photoreceptors. J. Neurosci. 21, 6745–6757.

Doerre, G., Malicki, J., 2002. Genetic analysis of photoreceptor cell development in the zebrafish retina. Mech. Dev. 110, 125–138.

Driever, W., Solnica-Krezel, L., Schier, A.F., Neuhauss, S.C., Malicki, J., Stemple, D.L., Stainier, D.Y., Zwartkruis, F., Abdelilah, S., Rangini, Z., Belak, J., Boggs, C., 1996. A genetic screen for mutations affecting embryogenesis in zebrafish. Development 123, 37–46.

Dryja, T.P., McGee, T.L., Reichel, E., Hahn, L.B., Cowley, G.S., Yandell, D.W., Sandberg, M.A., Berson, E.L., 1990. A point mutation of the rhodopsin gene in one form of retinitis pigmentosa. Nature 343, 364–366.

Dyer, M.A., Cepko, C.L., 2000. p57(Kip2) regulates progenitor cell proliferation and amacrine interneuron development in the mouse retina. Development 127, 3593–3605.

Famiglietti, E.V., 1991. Synaptic organization of starburst amacrine cells in rabbit retina: analysis of serial thin sections by electron microscopy and graphic reconstruction. J. Comp. Neurol. 309, 40–70.

Fujii, R., 2000. The regulation of motile activity in fish chromatophores. Pigment Cell Res. 13, 300–319.

Galli-Resta, L., Resta, G., Tan, S.S., Reese, B.E., 1997. Mosaics of islet-1-expressing amacrine cells assembled by short-range cellular interactions. J. Neurosci. 17, 7831–7838.

Germana, A., Gonzalez-Martinez, T., Catania, S., Laura, R., Cobo, J., Ciriaco, E., Vega, J.A., 2004. Neurotrophin receptors in taste buds of adult zebrafish (*Danio rerio*). Neurosci. Lett. 354, 189–192.

Haffter, P., Granato, M., Brand, M., Mullins, M.C., Hammerschmidt, M., Kane, D.A., Odenthal, J., van Eeden, F.J., Jiang, Y.J., Heisenberg, C.P., Kelsh, R.N., Furutani-Seiki, M., Vogelsang, E., Beuchle, D., Schach, U., Fabian, C., Nusslein-Volhard, C., 1996. The identification of genes with unique and essential functions in the development of the zebrafish, *Danio rerio*. Development 123, 1–36.

Ho, R.K., Kane, D.A., 1990. Cell-autonomous action of zebrafish spt-1 mutation in specific mesodermal precursors. Nature 348, 728–730.

Hu, M., Easter, S.S., 1999. Retinal neurogenesis: the formation of the initial central patch of postmitotic cells. Dev. Biol. 207, 309–321.

Kainz, P.M., Adolph, A.R., Wong, K.Y., Dowling, J.E., 2003. Lazy eyes zebrafish mutation affects Muller glial cells, compromising photoreceptor function and causing partial blindness. J. Comp. Neurol. 463, 265–280.

Kijas, J.W., Cideciyan, A.V., Aleman, T.S., Pianta, M.J., Pearce-Kelling, S.E., Miller, B.J., Jacobson, S.G., Aguirre, G.D., Acland, G.M., 2002. Naturally occurring rhodopsin mutation in the dog causes retinal dysfunction and degeneration mimicking human dominant retinitis pigmentosa. Proc. Natl. Acad. Sci. U. S. A. 99, 6328–6333.

Kimmel, C.B., Ballard, W.W., Kimmel, S.R., Ullmann, B., Schilling, T.F.,

1995. Stages of embryonic development of the zebrafish. Dev. Dyn. 203, 253–310.
Kolb, H., 1997. Amacrine cells of the mammalian retina: neurocircuitry and functional roles. Eye 11 (Pt. 6), 904–923.
Li, S., Mo, Z., Yang, X., Price, S.M., Shen, M.M., Xiang, M., 2004. Foxn4 controls the genesis of amacrine and horizontal cells by retinal progenitors. Neuron 43, 795–807.
Livesey, F.J., Cepko, C.L., 2001. Vertebrate neural cell-fate determination: lessons from the retina. Nat. Rev., Neurosci. 2, 109–118.
MacNeil, M.A., Masland, R.H., 1998. Extreme diversity among amacrine cells: implications for function. Neuron 20, 971–982.
MacNeil, M.A., Heussy, J.K., Dacheux, R.F., Raviola, E., Masland, R.H., 1999. The shapes and numbers of amacrine cells: matching of photofilled with Golgi-stained cells in the rabbit retina and comparison with other mammalian species. J. Comp. Neurol. 413, 305–326.
Malicki, J., 2000. Harnessing the power of forward genetics-analysis of neuronal diversity and patterning in the zebrafish retina. Trends Neurosci. 23, 531–541.
Malicki, J., Neuhauss, S.C., Schier, A.F., Solnica-Krezel, L., Stemple, D.L., Stainier, D.Y., Abdelilah, S., Zwartkruis, F., Rangini, Z., Driever, W., 1996. Mutations affecting development of the zebrafish retina. Development 123, 263–273.
Mariani, A.P., Hersh, L.B., 1988. Synaptic organization of cholinergic amacrine cells in the rhesus monkey retina. J. Comp. Neurol. 267, 269–280.
Marquardt, T., Ashery-Padan, R., Andrejewski, N., Scardigli, R., Guillemot, F., Gruss, P., 2001. Pax6 is required for the multipotent state of retinal progenitor cells. Cell 105, 43–55.
Martin, S.C., Marazzi, G., Sandell, J.H., Heinrich, G., 1995. Five Trk receptors in the zebrafish. Dev. Biol. 169, 745–758.
Maures, T., Chan, S.J., Xu, B., Sun, H., Ding, J., Duan, C., 2002. Structural, biochemical, and expression analysis of two distinct insulin-like growth factor I receptors and their ligands in zebrafish. Endocrinology 143, 1858–1871.
McNiven, M.A., Porter, K.R., 1986. Microtubule polarity confers direction to pigment transport in chromatophores. J. Cell Biol. 103, 1547–1555.
Morrow, E.M., Furukawa, T., Lee, J.E., Cepko, C.L., 1999. NeuroD regulates multiple functions in the developing neural retina in rodent. Development 126, 23–36.
Mullins, M.C., Hammerschmidt, M., Haffter, P., Nusslein-Volhard, C., 1994. Large-scale mutagenesis in the zebrafish: in search of genes controlling development in a vertebrate. Curr. Biol. 4, 189–202.
Murphy, D.B., Tilney, L.G., 1974. The role of microtubules in the movement of pigment granules in teleost melanophores. J. Cell Biol. 61, 757–779.
Neuhauss, S.C., Biehlmaier, O., Seeliger, M.W., Das, T., Kohler, K., Harris, W.A., Baier, H., 1999. Genetic disorders of vision revealed by a behavioral screen of 400 essential loci in zebrafish. J. Neurosci. 19, 8603–8615.
Ohnuma, S., Harris, W.A., 2003. Neurogenesis and the cell cycle. Neuron 40, 199–208.
Pelegri, F., 2002. Mutagenesis. In: Nusslein-Volhard, Dahm, R. (Eds.), Zebrafish, A Practical Approach. Oxford Univ. Press, Oxford, pp. 145–174.
Politi, L.E., Rotstein, N.P., Salvador, G., Giusto, N.M., Insua, M.F., 2001. Insulin-like growth factor-I is a potential trophic factor for amacrine cells. J. Neurochem. 76, 1199–1211.
Pujic, Z., Malicki, J., 2001. Mutation of the zebrafish glass onion locus causes early cell-nonautonomous loss of neuroepithelial integrity followed by severe neuronal patterning defects in the retina. Dev. Biol. 234, 454–469.
Reh, T., 1987. Cell-specific regulation of neuronal production in the larval frog retina. J. Neurosci. 7, 3317–3324.
Reh, T., Tully, T., 1986. Regulation of tyrosine hydroxylase-containing amacrine cell number in larval frog retina. Dev. Biol. 114, 463–469.
Ren, J.C., Stubbs Jr., E.B., Matthes, M.T., Yasumura, D., Naash, M.I., LaVail, M.M., Peachey, N.S., 2001. Retinal degeneration in the nervous mutant mouse: IV. Inner retinal changes. Exp. Eye Res. 72, 243–252.
Rickman, D.W., Rickman, C.B., 1996. Suppression of trkB expression by antisense oligonucleotides alters a neuronal phenotype in the rod pathway of the developing rat retina. Proc. Natl. Acad. Sci. U. S. A. 93, 12564–12569.
Schmitt, E.A., Dowling, J.E., 1999. Early retinal development in the zebrafish, *Danio rerio*: light and electron microscopic analyses. J. Comp. Neurol. 404, 515–536.
Seeliger, M.W., Rilk, A., Neuhauss, S.C., 2002. Ganzfeld ERG in zebrafish larvae. Doc. Ophthalmol. 104, 57–68.
Semple-Rowland, S.L., Lee, N.R., Van Hooser, J.P., Palczewski, K., Baehr, W., 1998. A null mutation in the photoreceptor guanylate cyclase gene causes the retinal degeneration chicken phenotype. Proc. Natl. Acad. Sci. U. S. A. 95, 1271–1276.
Solnica-Krezel, L., Schier, A., Driever, W., 1994. Efficient recovery of ENU-induced mutations from the zebrafish germline. Genetics 136, 1–20.
Sugimoto, M., 2002. Morphological color changes in fish: regulation of pigment cell density and morphology. Microsc. Res. Tech. 58, 496–503.
Tsujikawa, M., Malicki, J., 2004a. Intraflagellar transport genes are essential for differentiation and survival of vertebrate sensory neurons. Neuron 42, 703–716.
Tsujikawa, M., Malicki, J., 2004b. Analysis of photoreceptor development and function in zebrafish retina. Int. J. Dev. Biol. 48, 925–934.
Vaney, D.I., 1999. Neuronal coupling in the central nervous system: lessons from the retina. Novartis Found. Symp. 219, 113–125 (discussion 125-33).
Westerfield, M., 2000. The Zebrafish Book. University of Oregon Press, Eugene.
White, M.P., Gorrin, G.M., Mullen, R.J., LaVail, M.M., 1993. Retinal degeneration in the nervous mutant mouse: II. Electron microscopic analysis. J. Comp. Neurol. 333, 182–198.
Wong, K., 2005. Glutamatergic Mechanisms in the Outer Retina of Larval Zebrafish. Harvard University, Cambridge.
Yamada, E.S., Dmitrieva, N., Keyser, K.T., Lindstrom, J.M., Hersh, L.B., Marshak, D.W., 2003. Synaptic connections of starburst amacrine cells and localization of acetylcholine receptors in primate retinas. J. Comp. Neurol. 461, 76–90.
Yazulla, S., Studholme, K.M., Pinto, L.H., 1997. Differences in the retinal GABA system among control, spastic mutant and retinal degeneration mutant mice. Vision Res. 37, 3471–3482.